# X-ray bursts as a tool to constrain the equation of state of the ultra-dense matter inside neutron stars

Joonas Nättilä
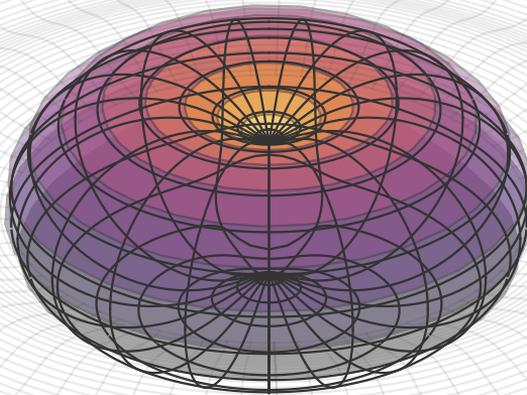
University of Turku

Faculty of Mathematics and Natural Sciences
Department of Physics and Astronomy

Supervised by

Prof. Juri Poutanen
Tuorla Observatory
University of Turku
Finland

Dr. Jari Kajava
Tuorla Observatory
University of Turku
Finland

Dr. Sergey Tsygankov
Tuorla Observatory
University of Turku
Finland

Reviewed by

Prof. Frederick K. Lamb
Department of Physics
University of Illinois at Urbana-Champaign
USA

Dr. Jean in 't Zand
SRON Netherlands Institute for Space Research
Netherlands

Opponent

Prof. Edward Brown
Department of Physics and Astronomy
Michigan State University
USA

List of publications

Modeling of neutron star atmospheres and emergent radiation

Paper I. Nättilä, J., Suleimanov, V. F., Kajava, J. J. E., Poutanen, J.: *Models of neutron star atmospheres enriched with nuclear burning ashes*, 2015, A&A, 581:A83, `http://dx.doi.org/10.1051/0004-6361/201526512`

Paper II. Nättilä, J. Pihajoki, P.: *Radiation from rapidly rotating oblate neutron stars*, 2017, A&A, submitted, `https://arxiv.org/abs/1709.07292`

Understanding the astrophysical environments of X-ray bursts

Paper III. Poutanen, J., Nättilä, J., Kajava, J. J. E., Latvala, O.-M., Galloway, D. K., Kuulkers, E., Suleimanov, V. F.: *The effect of accretion on the measurement of neutron star mass and radius in the low-mass X-ray binary 4U 1608-52*, 2014, MNRAS, 442:3777–3790, `http://dx.doi.org/10.1093/mnras/stu1139`

Paper IV. Kajava, J. J. E., Nättilä, J, Latvala, O.-M., Pursiainen, M., Poutanen, J., Suleimanov, V. F., Revnivtsev, M. G., Kuulkers, E., Galloway, D. K.: *The influence of accretion geometry on the spectral evolution during thermonuclear (type I) X-ray bursts*, 2014, MNRAS, 445:4218–4234, `http://dx.doi.org/10.1093/mnras/stu2073`

Constraining the mass, radius, and composition of neutron stars

Paper V. Nättilä, J., Steiner, A. W., Kajava, J. J. E., Suleimanov, V. F., Poutanen, J.: *Equation of state constraints for the cold dense matter inside neutron stars using the cooling tail method*, 2016, A&A, 591:A25, `http://dx.doi.org/10.1051/0004-6361/201527416`

Paper VI. Kajava, J. J. E., Nättilä, J., Poutanen, J., Cumming, A., Suleimanov, V., Kuulkers, E.: *Detection of burning ashes from thermonuclear X-ray bursts*, 2017, MNRAS, 464:L6–L10, `http://dx.doi.org/10.1093/mnrasl/slw167`

Paper VII. Nättilä, J., Miller, M. C., Steiner, A. W., Kajava, J. J. E., Suleimanov, V. F., Poutanen, J.: *Neutron star mass and radius measurements from atmospheric model fits to X-ray burst cooling tail spectra*, 2017, A&A, in press, `https://arxiv.org/abs/1709.09120`

Additional publications not included in the thesis

Kuuttila, J., Kajava, J. J. E., Nättilä, J., Motta, S. E., Sanchez-Fernandez, C., Kuulkers, E., Cumming, A., Poutanen, J.: *Flux decay during thermonuclear X-ray bursts analysed with the dynamic power-law index method*, 2017, A&A: 604:A77, `http://dx.doi.org/10.1051/0004-6361/201730823`

Kajava, J. J. E., Koljonen, K. I. I., Nättilä, J., Suleimanov, V., Poutanen, J.: *Variable spreading layer in 4U 1608-52 during thermonuclear X-ray bursts in the soft state*, 2017, MNRAS, 472:78-89, `http://dx.doi.org/10.1093/mnras/stx1963`

Suleimanov, V. F., Poutanen, J., Nättilä, J., Kajava, J. J. E.; Revnivtsev, M. G., Werner, K.: *The direct cooling tail method for X-ray burst analysis to constrain neutron star masses and radii*, 2017, MNRAS, 466:906-913, `http://dx.doi.org/10.1093/mnras/stw3132`

Suleimanov, V. F., Kajava, J. J. E., Molkov, S. V., Nättilä, J., Lutovinov, A. A., Werner, K. Poutanen, J.: *Basic parameters of the helium accreting X-ray bursting neutron star in 4U 1820-30*, 2017, MNRAS, 472:3905-3913, `https://10.1093/mnras/stx2234`

Abstract

Neutron stars are one of the most dense objects in the Universe. However, the exact description of the equation of state (EoS) of the cold ultra-dense matter inside them is still a mystery. In this thesis, we measure the size of some neutron stars using astrophysical observations of X-ray bursts that are produced by thermonuclear runaways in the uppermost layers of the star. By measuring the size, we can then set constraints on the nuclear physics of the interiors and ultimately on the EoS of the cold dense matter.

The size measurements are done by comparing the cooling of the neutron star surfaces after the bursts to theoretical atmosphere model calculations. Hence, accurate modeling of the emergent radiation from the atmospheres is needed. In the first part of this thesis, I have studied how the emergent spectra differ if the atmosphere is enriched with nuclear burning ashes from the bursts. This gives us new tools to understand and interpret the X-ray burst observations. In addition, I have shown how the emerging radiation is modified when it originates from rapidly rotating oblate neutron stars.

Furthermore, we must also be careful in selecting only those bursts that are not influenced by the infalling material. In the second part of the thesis, I have focused on studying the astrophysical environments of the X-ray bursts in order to quantify the effect of accretion on the mass and radius measurements. Importantly, it is shown that only the bursts that occur during the low-accretion-rate (hard) state can be used for the size determination because otherwise the accretion flow might influence the cooling of the stellar surface.

After taking these steps into account, it is possible to set constraints on the mass, radius, distance, and atmosphere composition of neutron stars exhibiting X-ray bursts. In the third part of the thesis, I have used the aforementioned models and methods to constrain the mass and radius of neutron stars using the hard state X-ray bursts. The method has been applied to three neutrons stars in low-mass X-ray binary systems 4U 1702−429, 4U 1724−307, and SAX J1810.8−260 for which the radius is measured to be between $10.9 - 12.4\,\mathrm{km}$ (68% credibility). The newly computed atmosphere models have also been used to detect a presence of burning ashes in the atmosphere of the neutron star in HETE J1900.1−2455. Later on, an improved Bayesian method of fitting the atmosphere models directly to the observed spectra has also improved the radius constraints of 4U 1702−429 to $R = 12.4 \pm 0.4\,\mathrm{km}$ (68% credibility). These results are in a good agreement with the current nuclear physical predictions and demonstrate how astrophysical measurements can be used to gauge the unknown nuclear physics of neutron stars.

Tiivistelmä

Neutronitähdet ovat universumimme tiheimpiä tähtiä. Niiden sisältämän erittäin tiheän kylmän aineen tilanyhtälö ja tarkka käyttäytyminen ovat kuitenkin vielä tuntemattomia. Tässä väitöskirjassa näytän kuinka kaukaisenkin neutronitähden koko voidaan mitata hyödyntäen niin kutsuttujen röntgenpurkausten lähettämää säteilyä. Röntenpurkaukset saavat alkunsa termisestä fuusioreaktiosta joka tuottaa valtaisan räjähdyksen tähden pintakerroksissa. Mittaamalla ja mallintamalla näistä purkauksista syntyvää säteilyä, saamme tietoa neutronitähtien sisältämän aineen käyttäytymisestä ja siten myös kylmän tiheän aineen tilanyhtälöstä.

Mittaukset tehdään vertaamalla neutronitähtien pinnalta alkunsa saavaa säteilyä teoreettisiin ilmakehämalleihin jotka ennustavat kuinka pinnan tulisi jäähtyä purkausten jälkeen. Tämän takia tarvitsemme tarkkoja malleja säteilyn kulusta ilmakehässä. Ensimmäisessä osassa väitöskirjaani olen tutkinut kuinka ilmakehässä olevat raskaat fuusioreaktioissa syntyneet alkuaineet vaikuttavat tämän säteilyn etenemiseen ilmakehän plasmassa. Tämä auttaa meitä ymmärtämään ja tulkitsemaan myös röntgenpurkauksista tehtyjä havaintoja. Lisäksi olen näyttänyt kuinka havaittu säteily muuttuu, kun se saa alkunsa erittäin nopeasti pyörivästä ja navoiltaan litistyneestä neutronitähdestä.

Tarkkojen ilmakehämallien lisäksi meidän täytyy myös ymmärtää mitä neutronitähden ympärillä tapahtuu. Väitöskirjani toisessa osassa tutkin kuinka ympäristö voi vaikuttaa herkkiin tähden säteen mittauksiin, koska joskus neutronitähden pinnalle putoava materia voi häiritä mittauksia. Tärkein löydöksemme on, että säteen luotettavaan mittaamiseen voidaan käyttää vain sellaisia purkauksia, jotka tapahtuvat kun putoavaa materiaa on erittäin vähän.

Kun edellä mainitut seikat huomioidaan on mahdollista mitata neutronitähden koko, etäisyys, ja ilmakehän koostumus vertaamalla oikeiden, havaittujen röntgenpurkausten jäähtymistä mallien ennusteisiin. Viimeisessä osassa väitöskirjaani olen tutkinut kolmen eri neutronitähden röntgenpurkausten säteilyä. Kyseiset neutronitähdet sijaitsevat kaksoistähtijärjestelmissä 4U 1702−429, 4U 1724−307, ja SAX J1810.8−260. Kyseisten neutronitähtien säde on mittauksieni mukaan 10.9 ja 12.4 km välillä (68% luottamustaso). Uusien ilmakehämallien avulla olemme myös todistaneet, että kaksoistähtijärjestelmässä HETE J1900.1−2455 sijaitsevan neutronitähden pintakerrokset sisältävät fuusioreaktion aikana syntyneitä raskaita alkuaineita. Kehitin myös uudenlaisen Bayesilaisen metodin, jossa ilmakehämalleja voidaan sovittaa suoraan röntgenpurkauksista tehtyihin havaintoihin. Tätä metodia käyttäen mittasin 4U 1724−429:ssä sijaitsevan neutronitähden säteeksi $R = 12.4 \pm 0.4$ km (68% luottamustaso). Nämä uudet tulokset ovat sopusoinnussa uusien ydinfysikaalisten ennusteiden kanssa. Lisäksi ne näyttävät kuinka astrofysikaalisia mittauksia voidaan käyttää apuna ydinfysiikan tutkimuksessa.

Acknowledgements

Contents

1 | Introduction

Neutron stars are curious objects encompassing many problems of modern physics and astrophysics still unsolved. Their unique nature makes them ideal laboratories for many of the most energetic phenomena in space. Born from the ashes of a supernova, they begin their life only when a normal star fades away and dies in a spectacular explosion.From there on, they continue their life by slowly collecting the surrounding interstellar matter or by devouring an unlucky companion star located next to them. It is not the $\sim 10^{30}$ kilograms they weigh but the sphere mere ~ 10 km in radius that they encapsulate this material into that is then able to bend spacetime itself. Such an impressive feat award them a categorization of a special stellar group called *compact objects*. Along with white dwarfs and black holes, these strange compact objects have been under scientific scrutiny for almost nine decades. Still, one fundamental question remains: What are neutron stars made of?

In the next few sections, we will discuss these peculiar objects habitating the space around us in detail. First, a short history of their discovery is given, followed by simple physical arguments on why we actually expect them to exist in the first place. This will hopefully help us in building some intuition about physical phenomena possible near and inside these stars.

1.1 Short history

1.1.1 From imagination to reality

In 1908, Lev Landau was born in Baku, Azerbaijan. Landau turned out to become a brilliant Soviet scientist, who already at the age of 14 matriculated at the Baku State University studying simultaneously in both the Department of Physics and Mathematics and the Department of Chemistry. Soon after, he became disinterested in chemistry but continued to be fascinated by physics throughout his whole career. In 1931, at the age of 23, Landau published an exceptional paper where he speculated on the existence of stars containing matter at nuclear densities:[1]

> *...the density of matter becomes so great that atomic nuclei come in close contact, forming one gigantic nucleus.*

What made this paper exceptional was that it was written before the existence of neutrons was confirmed. For contemporary science, this meant a violation of quantum mechanics, since atoms were thought to consist of protons and electrons

only, and they certainly could not exist together in the same place inside such a hypothetical star. Nevertheless, it marked the first theoretical speculation on the existence of what we now know as neutron stars.

Landau needed not wait for long. Already next year, in 1932, James Chadwick confirmed that neutrons really were a fundamental part of our nuclear physics with his works dubbed *Possible Existence of a Neutron*[2] and the follow-up *Existence of a Neutron*[3]. His experimental findings then confirmed the theoretical predictions his supervisor Ernest Rutherford made already in 1920[4]. Later on, in 1935, Chadwick was awarded the Nobel Prize in Physics for his findings. Chadwick himself continued his career as part of the Manhattan project, as it was basically his groundbreaking work that inspired the U.S. government to begin serious research into the atomic bomb.

Now that the existence of the neutron was confirmed, it did not take long for others, independent of Landau, to propose similar stars. At the Meeting of the American Physical Society at Standford in December 1933, one year after the neutron discovery, Wilhelm Baade and Frank Zwicky made their famous proposal that Supernovae should be considered a new category of astronomical objects.[5,6] At the same time, they also stated:

> *...we advance the view that a super-nova represents the transition of an ordinary star into a neutron star, consisting mainly of neutrons. Such a star may possess a very small radius and an extremely high density.*

Such statements were, however, deemed a work of imagination by a bunch of weird astronomers. Zwicky, on the other hand, kept on insisting that neutron stars really are out there. Much later on, A.G.W. Cameron, a former post-doc at Caltech (where Zwicky was also situated) during 1959–1969, recalls:

> *For years Fritz [Zwicky] had been pushing his ideas about neutron stars to anyone who would listen and had been universally ignored. I believe that the part of the problem was his personality, which implied strongly that people were idiots if they did not believe in neutron stars.*
> (A.G.W. Cameron, 1999)

Progress on the theoretical understanding of neutron stars was also tightly connected to understanding the interiors of white dwarfs. Unlike the mysterious nuclear forces related to neutrons, the physics of white dwarfs was more related to understanding the behavior of electrons. A breakthrough in this field came in 1925, when a young Paul Dirac formulated the quantum wave equations for the motion of electrons[7]. What soon followed was a description of the pressure of degenerate electron gas by Ralph Fowler, Dirac's supervisor[8]. The implications were severely against the previously known physics; even in zero temperature, there would be a degeneracy pressure preventing matter from collapsing due to the exclusion principle of quantum mechanics.

Using a simplified uniform density approximation, Edmund Stoner was then able to show that this implied a maximum mass limit for white dwarfs.[9] Thus, a surprising result was obtained: when the density of a white dwarf approaches infinity, the mass reaches a maximum value. The German-Estonian Wilhelm Anderson later realized that the electrons in this problem must actually be treated relativistically[10], something overlooked by Stoner. Anderson tried to correct the crude mistake by deriving the equation of the state of relativistic degenerate electron gas but ended up making severe mistakes. It was Stoner who corrected his equations based on communication with Anderson and re-derived his maximum mass limit. Regardless of Stoner's efforts, it was later named Chandrasekhar's mass limit for its importance in astrophysics.

This was to honor Subrahmanyan Chandrasekhar, a young and prolific Indian physicist and astrophysicist, who was working on the same topic after reading Fowler's paper on degenerate electron gas. Unlike Stoner's limit computed using the uniform density approximation, Chandrasekhar realized that a polytropic density profile is a more physical albeit mathematically more challenging formulation. Still, the 19-year-old Chandrasekhar, already known for his mathematical prowess, was able to integrate the equations numerically by hand and obtained a similar limiting mass[11]. Later on, however, it has been found that Chandrasekhar was not even the second person to derive the mass limit, but the third:[12] the Soviet physicist Yakov Frenkel published a similar derivation, independently and unknowingly of the progress in the west, in which he applied the relativistic degenerate electron gas results to white dwarfs and concluded that an upper limit on the mass must exist[13]. However, his work went by unnoticed.

Nevertheless, the maximum mass for a white dwarf had been laid out, and in the end, after all the relevant physical inclusions, it turned out to be 1.44 $M_\odot$, or 1.44 times the mass of our Sun. What makes this limit important for us, is that the maximum mass for a white dwarf is related to the minimum mass for a neutron star, an important connection first made by George Gamow in 1939[14]. The idea behind it is simple: if the degenerate electron gas pressure, quantum mechanical in nature, is what keeps the white dwarfs from collapsing, what happens when the maximum mass is reached and even this strange pressure is unable to resist the forces of gravity? At a conference in Paris in 1939, Chandrasekhar laid out the answer:

> *If the degenerate core attains sufficiently high densities, the protons and electrons will combine to form neutrons. This would cause a sudden diminution of pressure resulting in the collapse of the star to a neutron core.*

A neutron star should thus have a mass smaller than the Chandrasekhar limit, i.e. $M \sim 1.44\,M_\odot$, and consist of neutrons only, exactly like proposed by Landau eight years earlier without the knowledge of neutrons, or later on by Baade and Zwicky when they presented their theory of supernovae!

It was before the Second World War that a solid basis for a theory of neutron

stars was established. This was, however, just the beginning. The next question would be the critical one that we are still trying to answer today: if they exist, how big are they? The problem was that because of the extremely dense nature of these objects, the classical stellar equilibrium equations were no longer valid, and thus it was not possible to even estimate the size of a neutron star. The problem was unwieldy due to its general relativistic nature; the immense mass of the neutron star was bending spacetime itself, and the more compact it was, the more it could bend it. On the other hand, the more curved spacetime was, the more the star would gain weight and the more compact it would become.

It was already during the same year as Gamow's remark, in 1939, that a theoretical framework for studying this problem was published. This was done independently by Richard Tolman[15] and Robert Oppenheimer together with his student George Volkoff[16]. Both papers were even submitted on the same day, the 3rd of January, to Physical Review and were published on the same February issue. More importantly, they both described a hydrostatic equilibrium for a spherically symmetric object in general relativity, exactly what was needed to study neutron stars. Because of its great importance, the solution is now known as the Tolman-Oppenheimer-Volkoff equation. In addition, Oppenheimer and Volkoff applied their equation and numerically calculated the structure of a neutron star consisting of non-interacting strongly degenerate neutron gas. This marked the very first attempt in characterizing neutron stars. Similar to white dwarfs, they also obtained an upper limit for their mass. However, as a disappointment for everyone, it was calculated to be around $0.7\,\mathrm{M_\odot}$, i.e. less than the Chandrasekhar limit of $1.44\,\mathrm{M_\odot}$ for white dwarfs, indicating that neutron stars could not exist in nature. It took almost two more decades to show that it was actually the assumption of no interaction between the neutrons that was causing this hiccup.

Moreover, it was actually not Tolman nor Oppenheimer and Volkoff who first discovered the general relativistic hydrostatic equation. It was now Chandrasekhar's turn to avoid having an important result credited to him; together with John Von Neumann, Chandrasekhar extended his work on white dwarfs to also cover neutron stars and in the process derived exactly the same equilibrium equation in 1934, five years before the groundbreaking publication of Tolman, Oppenheimer and Volkoff.[17] It is, however, worth mentioning that later on, in 1983, Chandrasekhar received the Nobel Prize in Physics for his work on "theoretical studies of the physical processes of importance to the structure and evolution of the stars". So he certainly received at least some credit for his important work.

Around the same time, in 1937, Gamow and Landau also independently proposed that the accretion of matter onto a dense neutron star core could be the missing source of energy for stars. This increased the interest towards neutron stars, and the field flourished in the 1930s. However, it was soon shown that stars are powered not by accretion but by thermonuclear reactions as first suggested in the 1920s by Sir Arthur S. Eddington.[18] The interest in neutron stars then faded away and the research focused on weaponizing the nuclear forces.

The next big breakthrough came almost 20 years later in the 1950s, when

John Wheeler and his collaborators constructed the first realistic equation of the state of dense matter[19]. For the outer layers, known as the crust, they applied a semi-empirical mass formula together with the equation of the state of degenerate electrons. For the dense core, they assumed a mixture of three ideal Fermi gases composed of neutrons, protons, and electrons. This marked the first consistent formulation of neutron star structure. It was followed by Cameron, who applied the Skyrme equation of state for the high-density matter.[20] This had important implications, as he was then able to show that the nuclear forces stiffen the matter considerably in comparison to the non-interacting free neutrons. Similar to Tolman and Volkoff, he then went to calculate the maximum possible mass of a neutron star and arrived at approximately $2\,M_\odot$. This was an important theoretical breakthrough as it implied that neutron stars can, after all, exist. A new wave of interest towards neutron stars was thus launched as everybody wanted to observe them.

1.1.2 Many observational faces of neutron stars

After Wheeler and Cameron had laid the modern foundation for studies on neutron star structure, everyone was eager to find these strange objects in the night sky. It did not take long before researchers realized that as neutron stars are born in the supernova explosions, we expect them to be hot. Most of the theoretical effort in the 60s was then focused on developing models for the cooling of neutron stars.[21–27] It was the potential thermal radiation from this cooling that could then be used to detect them, as was first shown by Hong-Yee Chiu[22]. The first calculations predicted surface temperatures of $T \sim 10^6$ K for a neutron star of the age of around 1000 years. This had important implications for the observers as it meant that neutron stars would mainly radiate in the range of X-rays. The atmosphere of Earth, on the other hand, was impenetrable to the X-ray wavelengths. Luckily, the 60s also marked the beginning of a golden era for spaceborn observatories.

Since X-rays could not reach the surface of the Earth, humankind went into space to observe them. In the late 1950s and early 1960s, it was the pioneering experiments of the Italian-American astrophysicist Riccardo Giacconi that opened this new window into the Universe. Giacconi first started with rocket-borne experiments and later continued by leading the development of the first orbiting X-ray satellite Uhuru, "*freedom*" in Swahili.[28] After the first X-ray satellite, Giacconi continued with the Einstein Observatory, the first fully imaging X-ray satellite, and later with the Chandra X-ray observatory. For all of his efforts, he received the Nobel Prize in Physics in 2002 "for pioneering contributions to astrophysics, which have led to the discovery of cosmic X-ray sources".

During the starting boom, several extra-terrestrial X-ray sources were discovered. As is common in science, the first discovery actually came by accident. A team led by Giacconi launched an Aerobee 150 rocket to the skies in June 1962 with a payload of a highly sensitive soft X-ray detector meant to observe the X-rays from the Moon. Due to a slight change (or a mistake) in the planned trajectory, it ended up observing the constellation of Scorpius and caught a glimpse of what is

now known as the first extraterrestrial X-ray source, Sco X-1. Little did they know that this was actually the first neutron star radiating towards us. Five years later, in 1967, Iosif Shklovsky was the first to propose that Scorpius X-1 is a neutron star[29], but his work attracted little to no attention.

The first deliberate searches of neutron stars were aimed at the Crab Nebula, a well-known candidate for hosting a neutron star. The Crab Nebula, already known in the 1920s and 1930s to be a supernova remnant is known to have exploded exactly on the 4th of July, 1054.[30–33] In contemporary Chinese, Japanese, and Arab history writings, a "guest star" is described to appear in the constellation of Taurus and to persist even in broad daylight for 23 consecutive days. Even after that, it remained visible in the night sky for two years. For astronomers, this was a clear sign of a nearby supernova going off.

But it was not only the spectacular supernova but what was left behind that eluded astronomers. Already in 1942, our old friends Baade and Rudolf Minkowski correctly found that the center of the Crab Nebula contained an unusual star.[34,35] In the following years, the mystery gained depth when a radio emission was also detected.[36] This gathered a lot of interest from the theorists, as they were trying to explain the origin of the energy powering the nebula. In 1953, Shklovsky was on the right track again when he predicted that the emission is due to synchrotron radiation from relativistic electrons spiraling along magnetic field lines. His predictions were further strengthened in the next year 1954, when Victor Dombrovsky discovered that the optical radiation from the Crab nebula is polarized,[37] as it should be if the radiation originates from synchrotron process. The next piece of the puzzle came in 1964, when Lodewijk Woltjer, who did his PhD on the Crab Nebula, argued, based on the conservation of magnetic flux, that neutron stars should have a strong magnetic field, enough to produce this synchrotron radiation.[38] Similar results were independently obtained in the East by Vitaly Ginzburg.[39]

Early X-ray telescopes of the time had a very poor angular resolution, so imaging the Crab Nebula to get an answer to the puzzle was difficult. The first observation in 1964 by S. Bowyer et al. used a clever method of partial lunar occultation to cover unwanted parts of the sky with the Moon, and what followed was the first X-ray observation of the neutron star candidate everybody was waiting for.[40] It was, however, followed by a disappointment when a follow-up observation measured the source size to be about 1 light-year in size (10^{13} km) in comparison to the 11 light-years of the whole nebula.[41] The result was much larger than what was expected for a neutron star that should be a mere ~ 10 km in radius. Ironically, what they did not know was that this was just as expected; for young neutron stars like the one in the Crab Nebula, a pulsar wind (consisting of charged particles similar to solar wind) is expected. This wind will then create a surrounding shell called a plerion, much bigger in size, around the neutron star, and this shell is the source of the X-rays. Hence, the mystery remained even though Nikolai Kardashev in the East and Franco Pacini in the West gave plausible pioneering explanations for the formation of the wind in 1964 and 1967, respectively.[42,43]

Despite all the efforts (and partly due to bad luck), no concrete observations supporting the existence of neutron stars still existed. This all changed in July 1967, in the farmlands near Cambridge. There, a pasture was filled with a primitive antenna consisting of wires hanging from stakes — a state-of-the-art radio antenna of those times. The idea was to use this newly build radio telescope to study interplanetary scintillation that could help in resolving quasars, another form of compact objects powered by black holes, from extended sources in the sky. Among several other students who were working for Anthony Hewish was a young PhD student named Jocelyn Bell. In addition to the signal from the scintillation, she discovered a deviation on her chart-recorded papers; an extremely regular signal with a period of 1.3373012 seconds caught Bell's attention. Originally, this was dubbed (partially as a joke) Little Green Men 1 (LGM-1). In reality, what they were seeing, Bell quickly realized, was the first pulsar, a rapidly rotating neutron star whose radio emission beam sometimes points towards us, like a distant lighthouse. More Little Green Men quickly followed, and by the end of the year 1968, dozens of LGMs were known. The finding was later published in the Nature of 1968 by Hewish et al.[44] Hewish's announcement was quickly followed by more than 100 papers on pulsars, speculating the possible origin of the signal. The winning argument came from Timothy Gold, who showed that pulsars are strongly magnetized rapidly rotating neutron stars.[45] However, one should not forget the similar seminal theoretical paper already made in 1967, before the discovery, by Pacini.[43] More proof came when our old friend the Crab Nebula was shown to host a pulsar rotating at a period of merely 33 milliseconds.[46] Anything but a neutron star would be destroyed by the centrifugal forces from such rotation.

The finding of Bell and Hewish was sensational and marked the first detection of a neutron star, almost 40 years after the theoretical speculation by Landau. Later on, Hewish was awarded the Nobel Prize in Physics in 1974 "for the discovery of pulsars", a somewhat unfair recognition taken into account that it was Bell who found them in practice. Hence, despite all the efforts in X-ray astronomy, the concluding evidence finally came from the radio wavelengths.

One should not, however, feel sorry for the X-ray astronomers, as they got their fair share of neutron-star-related revelations during the next decade. Important discoveries especially for studying the nature of accretion, or how matter infalls onto a compact object, came from the first long-duration observations done with the Dutch astronomy satellite ANS. As a direct competitor for the European ANS, the U.S. funded Los Alamos National Laboratory nuclear research center was also in the game of observing X-rays from compact objects. Their Vela satellites were sent to space mostly to monitor the compliance of the 1963 Partial Test Ban Treaty of nuclear weapons but they were used for science, too. In 1975, the ANS satellite was commissioned to study possible black holes in the center of globular clusters but happened to stumble upon something completely different; Short, ~60-second-long X-ray flares were detected from the globular cluster NGC 6624 by Grindlay and Heise.[47] The competing Los Alamos group found similar energetic bursts, but due to the poor angular resolution (collecting X-rays from the Earth was easy

and hence no effort was put in for a good spatial accuracy), they could not pin point the exact location of the sources.[48] Later on, Clark et al. went through the existing SAS-3 data from May 1975 and found a series of ten similar bursts from the same location, NGC 6624.[49] Even more retrospectively, it turned out that these strange flares had already been observed in 1969 from Cen X-4[50] with another Vela satellite and in 1971 with the Soviet Kosmos 428 X-ray detector[51]. Their nature, however, remained elusive.

Pioneering theoretical work on thermonuclear instabilities on the surface layers of accreting neutron stars was initiated by Hansen and van Horn in 1975.[52] They constructed stationary burning shells to lay on top of neutron stars but instead found out that most of them were actually unstable. The choice of word, unstable, might not convey the full weight of the physical issue though; such a layer on top of the surface of a neutron star burning uncontrollably meant a spectacular firework. Shortly after the Los Alamos results came in, an Italian astrophysicist Laura Maraschi was able to connect the dots while visiting MIT in February 1976 and speculated that these recently observed X-ray bursts were due to thermonuclear flashes on the surface of accreting neutron stars.[53,54] Woosley and Taam concluded similarly in their 1976 paper titled "Gamma-ray bursts from thermonuclear explosions on neutron stars".[55] Observational evidence soon followed when van Paradijs et al. and Thorstensen et al. were independently able to optically resolve the companions of two known bursting sources, Cen X-4[56] and Aql X-1[57]. Not only did these observations confirm that there is a companion star close by but also that it must be within such a close distance of the neutron star that accretion, i.e. a constant flow of new fuel for the explosions, can exist.

All of the aforementioned discoveries were, however, nothing but a prelude to what was discovered in the years to follow. We will end this short historical review by listing some of the most important more modern findings. A big revelation came in 1979 when a very intense burst of gamma rays was detected by two Soviet satellites, Venera 11 and Venera 12.[58] Later dubbed Soft Gamma Repeaters (SGRs), their energy source remained mysterious for decades. A theoretical breakthrough came in 1992 when Robert Duncan and Chistropher Thompson showed that the bursts, orders of magnitude stronger than the X-ray bursts, could originate from a neutron star with a magnetic field 100 to 1000 times more powerful than what was previously known.[59] Today, these neutron stars are more commonly known as magnetars, a subclass of young neutron stars where the initial magnetic field has been amplified by delicate dynamo processes during the supernova explosion. Another surprise came in 1982, when a team led by Donald Backer changed how we look at pulsars when, using the world's largest radiotelescope in Arecibo, they found a pulsar spinning 641 times per second.[60] This new neutron star was dubbed a millisecond pulsar, and unlike its predesessors, we now know that instead of slowly decreasing in spin, it belongs to a class of old pulsars that have been spun up by the accretion. In 2000, our understanding of the thermonuclear X-ray bursts was also changed when Cornelisse observed a very long, not minutes but hours long, burst from a neutron star normally exhibiting regular short bursts.[61] These

were then dubbed as superbursts, in contrast to normal ones. The reason for this difference is, we think, the burning material; normal bursts use hydrogen and helium as their fuel but superbursts can devour a carbon shell in a matter of hours if the conditions are just right.

1.2 From first principles to a neutron star

1.2.1 Background: Sun and stars

First, let us see what we can learn from neutron stars using simple estimates and conservation laws. Neutron stars are born from the death of a normal star. The most familiar one to us is our Sun, one Astronomical Unit or about 1.496×10^{13} cm away from us. With a mass of $M_\odot = 1.99 \times 10^{33}$ g and a radius of $R_\odot = 6.96 \times 10^{10}$ cm, our Sun gives us an idea of the typical stellar scale. Curiously, these numbers also mean that the mean density of the Sun is $\rho_\odot \approx 1.41 \, \mathrm{g \, cm^{-3}}$, only $1.4\times$ the density of water.

Like all stars, our Sun is held together by the inward-pulling gravity. Gravity does not prefer any direction more than another, and so a spherical object is expected to form. In addition to the inward-facing force, an outward-facing force is needed to balance the system. For normal stars this force originates from thermal gas pressure.

We observe stars in the night sky because they shine. This radiation originates from the thermonuclear fusion reactions inside the star. *Thermo* here refers to the temperature and heat, *nuclear* to the atomic nuclei, and *fusion* to a process where elements are fused together. During the thermonuclear fusion process, the star's core fuses light elements such as hydrogen into heavier ones like helium. The mass of four hydrogen atoms is more than a mass of one helium atom. This mass difference between the start and the end results is then transferred into energy in accordance to Einstein's famous $E = mc^2$ formula. A whole sequence of such fusion processes takes place inside the star, where lighter elements are merged together to build heavier and heavier elements. The energy release from this mass-to-energy conversion will then give the star a sufficient thermal pressure support to keep it from collapsing under the relentless gravity trying to squash it.

The fusion of elements does not continue forever. In the beginning, four protons collide to form an alpha particle[*] In the next stage, three helium nuclei collide to form carbon, and so on, until iron is created. Production of iron marks the end of the possible fusion chain, since the fusion of two iron atoms no longer releases energy. On the contrary, it requires external energy to take place.[†] This iron produced will then form a dead core without any energy output.

Like all big furnaces, at some point the star will run out of fuel to burn. What is left behind is an inner core of iron with subsequent onion-like layers of lighter and lighter elements. The crucial question to ask next is: what is supporting this iron

---

[*]Alpha particle consists of two protons and two neutrons, i.e., doubly ionized helium nuclei.

[†]This opens up another possibility of creating energy by splitting heavy elements, an inverse process to what is described here. Such a process is called fission and is familiarly taken advantage of in Earth's nuclear power plants.

core now that the thermal gas pressure from the fusion process is lost? This was the question that led scientists like Chandrasekhar to the realization of degenerate matter and white dwarf stars in the 1920s.

1.2.2   White dwarfs and quantum mechanics

The answer lies in the elusive quantum mechanics. When the atoms inside matter are packed close enough together, we need to apply wave-like characteristics for them instead of classical point-like thinking. Because of their smaller mass, the electrons orbiting the nuclei enter the realm of quantum mechanics first, in comparison to the heavier protons and neutrons in the atomic core. A freely moving electron confined into a small enough space because of its surrounding neighbors will start to attain only some fixed values of momenta. In physics, we speak about the quantization of energy levels. The reason for this is similar to a vibrating string of a guitar; a string fixed from both ends can only vibrate on some specific wave modes that are set by its length. An additional complication for the electrons is set by the Pauli exclusion principle, which forbids more than one electron to occupy the same wave mode or quantum state inside the same region. This gives rise to a degeneracy pressure as electrons fill their quantum states from the lowest to the highest, and can thus not be packed any tighter together. A star held together by this degeneracy pressure of its electrons is known as a white dwarf. From this setup, it only takes a short step into realizing the existence of neutron stars, because we can, once again, push forward and ask: what next?*

1.2.3   Neutron stars, at last

What if, at some point, even these quantum effects of the electrons are not enough to support the star? One does not need to worry, since after the lightweight electrons have given all they can, it is the heavy neutrons that slowly start to enter the quantum mechanical realm. In practice, the matter will turn into a one big team of neutrons because when the positive (+) central proton and the surrounding negative (−) electron come in contact, a neutral neutron is created.† The degeneracy pressure of such a neutron porridge is multiple orders of magnitude larger than what the electrons can offer, yielding an ultimate solution to the pressure support problem.

Let us consider the consequences of this thought experiment. More detailed calculations show that the resulting iron core sitting at the center of the star is weighing a maximum of around $\sim M_\odot$.‡ Hence, there are $M_{core}/m_{atom} \sim M_\odot/m_p \approx 1.99 \times 10^{33}$ g$/1.67 \times 10^{-24}$ g $\sim 10^{57}$ atoms trapped inside the core. § Here we are

---

*The reader can be assured that the chain of thermal pressure → charge repulsion → electron degeneracy will come to a halt as the final neutron degeneracy really is the last possible supporting force in nature (maybe excluding quark degeneracy pressure)

†In reality, the beta decay formula is $e^- + p = n + \bar{\nu}_e$, where the additional electron anti-neutrino is needed to preserve the quark color neutrality.

‡This is quite a reasonable-sounding assumption considering that the stars that explode are around $\sim 10\,M_\odot$ in size and we certainly do not expect everything to fall into the core.

§The mass of the atom, $m_{atom} = m_p + m_e$, is approximated (to an excellent accuracy) by considering the nuclei alone as the electron mass $m_e \approx 9.11 \times 10^{-28}$ g is negligible in comparison to the

already considering not iron atoms but pure hydrogen atoms only to simplify the presentation. Working backwards from these numbers, we can estimate the size of the compressed core. Using a typical radius of $r_n \approx 1.25 \times 10^{-13}$ cm for the nuclei, we would expect these particles to form an object of around $R \sim (10^{57})^{\frac{1}{3}} \times 1.25 \times 10^{-13}$ cm $\sim 10^6$ cm. Thus, we have ended up with a star consisting of only neutrons, with a size of ~10 km and a mass of ~1 $M_\odot$: a neutron star!

By considering simple order-of-magnitude estimates we have now ended up characterizing the dimensions of a typical neutron star. A canonical neutron star is often taken to have $R = 10$ km and $M = 1.4\,M_\odot$, so let us also adopt these numbers for the following considerations. Such dimensions give us an impressive mean density of $\rho \sim 7 \times 10^{14}$ g cm^{-3}. In comparison, for a typical nucleon (such as a neutron or a proton) we had $m_p \approx m_n \approx 1.67 \times 10^{-24}$ g and $r_n \approx 1.25 \times 10^{-13}$ cm, yielding us a nuclear density of $\rho_n \approx 2 \times 10^{14}$ g cm^{-3}. Not surprisingly, the densities are of similar magnitude. However, when comparing these numbers to our everyday matter, the difference is huge, almost 14 orders of magnitude; a cubic centimeter of water weighs 1 g, whereas the same volume of neutron star matter would weigh 100 000 000 000 000 g or 100 million metric tons.

Matter compressed to such a small volume has an extreme impact even on the surrounding spacetime. Let us try to estimate, again, the order of magnitude of these effects by considering the escape velocity — a velocity needed to escape the local gravitational pull of an object. For us, on the surface of the Earth, it turns out to be $v_\oplus = \sqrt{2GM_\oplus/R_\oplus} = 1.12 \times 10^6$ cm s^{-1}, for $M_\oplus = 5.97 \times 10^{27}$ g and $R_\oplus = 6.37 \times 10^8$ cm. Similarly, for the Sun it is $v_\odot = 6.18 \times 10^7$ cm s^{-1}, or 0.002× the speed of light. On the other hand, for a neutron star, we obtain $v_{NS} = 1.93 \times 10^{10}$ cm s^{-1}, which is already about half of the speed of light! Hence, relativistic effects become crucial to take into account when considering neutron stars, as one can not even escape from the surface of the star without velocities close to those of the light.

Let us next think about the possible spin rates that a neutron star can have. For our Sun, it takes about one month (or approximately 25.5 days, to be more exact) to revolve around itself, corresponding to a spin rate of 4.5×10^{-7} Hz. When compressed to the dimensions of a neutron star, the radius changes by a factor of $R_\odot/R_{NS} \approx 6.96 \times 10^{10}$ cm$/10^6$ cm $\sim 7 \times 10^4$. It is important to notice that when a rotating object collapses, it preserves its angular momentum, not the spin rate. Similar to an ice-figure skater pulling her arms inwards while spinning, we observe an increase in the spin in order to preserve the angular momentum. As the rotational inertia increases as a square from the distance to the axis, our Sun, when compressed to the scale of a neutron star, would obtain a spin of 4.5×10^{-7} Hz $\times (7 \times 10^4)^2 \sim 2 \times 10^3$ Hz, 2000 revolutions per second. The young proto neutron star, however, quickly slows down after its birth, so more typically, spins of around 100 to 1000 Hz are observed, which is still about one revolution per 1 to 10 milliseconds.

---

proton mass.

One final characteristic we can try to estimate is the magnetic field. Here we can follow a similar chain of reasoning as with the spin and start from typical values such as those of our Sun. For the Sun, the slow rotation gives rise to a dynamo process that produces a magnetic field of around $B_\odot \approx 1\,\text{G}$.[*] When considering magnetic field, it is the magnetic flux through the surface that conserves, hence we expect the field to scale also as a square of the radius. Using the same compression ratio of 7×10^4 for the radius, we then obtain $B_{\text{NS}} \approx 1 \times (7 \times 10^4)^2\,\text{G} \sim 10^{10}\,\text{G}$. Comparing this to the value of $10^6\,\text{G}$ for the strongest non-destructive magnet on Earth, we start to grasp the level of energetics that neutron stars have to offer; even their original non-amplified magnetic field is $\times 10\,000$ stronger. In some cases, a dynamo effect originating from the rapid rotation of the star can amplify the magnetic field even by a factor of a million. This gives rise to neutron stars with immense magnetic field strengths of $B \sim 10^{16}\,\text{G}$.

It is fair to conclude that neutron stars are dominating the record tables of physics in almost all of their aspects. They are *super*dense, *super*fast rotators, sources of *super*strong magnetic fields, and *super*rich in the range of physics involved. In short: they are the *super*stars of physics![†]

---

[*] A typical refrigerator magnet is about 50× stronger with a magnetic field of 50 G.

[†] This is (humorously) called the Pines theorem as everything is *super-* when considering neutron stars, as postulated by David Pines in a talk given at the conference on Neutron Stars: Theory and Observation (The NATO Advanced Study Institute, Crete, Greece, September 3–14, 1990).

2 | Physics of neutron star interiors

In this chapter, we will review the neutron star interiors in more detail. In practice, this means describing the behavior of the matter from densities of $\sim 10^{-3}\,\mathrm{g\,cm^{-3}}$ to $\sim 10^{15}\,\mathrm{g\,cm^{-3}}$, an impressive 18 orders of magnitude range starting from a hot and rarefied electron corona to an ultra-dense neutron liquid.

The structure of the star can be roughly divided into three distinct sections: atmosphere, crust, and core. These sections are visualized in Fig. 2.1. Neutron star atmosphere holds a negligible amount of matter in comparison to the whole star, but it plays an important role in shaping the outgoing radiation. It is the radiation from the atmosphere that we actually observe. The crust, like the name implies, can be understood as a solidified layer surrounding the liquid core. Physics describing the crust is relatively well known and same type of matter consisting of ions, protons, and electrons can be found inside white dwarf stars. Bulk of the mass, on the other hand, is located in the liquid neutron core. Detailed microphysics of such matter is still unknown, and this is reflected in a large uncertainty in the actual size of the star that is still poorly constrained.

We begin by giving an overview of the characteristics of each of the different layers. By combining this information, we can then build different models for the neutron stars and describe some more global aspects of them such as mass and radius. For this we need to solve the relativistic equations of hydrostatic equilibrium, that are also discussed. In the end, this enables us to build a mapping between the (un)known microphysics of the dense matter and the astrophysical observables.

2.1 Equation of state

In thermodynamics, we speak of *state variables* that describe a current state of the matter under given physical conditions. These include, for example, the density ρ, pressure P, and temperature T of the matter. Equation of state is a thermodynamical equation connecting these state variables together. Often, when focusing on neutron stars, what we mean by EoS is a function connecting the pressure and the density of the matter only, $P(\rho)$.

The dependency on the rest of the variables such as temperature can be often forgotten because the matter is *degenerate*. In contrast to the "normal" matter where statistical moments such as temperature can be used to describe a large ensemble of particles, the degenerate matter is dominated by quantum mechanical effects of single particles. Because of the immense densities, a free particle in de-
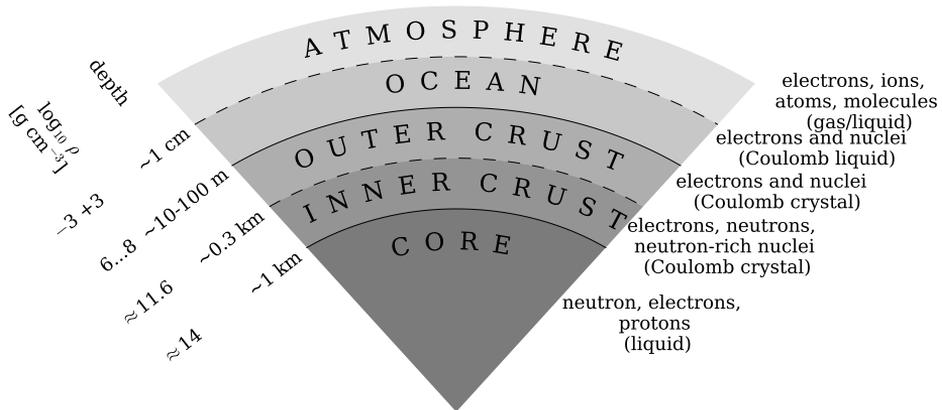
Figure 2.1: Schematic view of neutron star structure illustrating the different internal regions, related densities, and the compositions.

generate matter is actually bounded into a finite volume. Inside this small volume, the energy levels of the particle are restricted to take only a discrete set of values called quantum states, because of the underlying wave-nature of the quantum-mechanical description. Hence, a notion of temperature, for example, does not make much sense.

An overview of the EoS for the full range of densities relevant to neutron stars is shown in Fig. 2.2. From here it is easy to see that temperature only plays a role in the very uppermost ~10 meters of the stars interiors. Behavior of the matter is also quite well known all the way up to the crust-core interface, after which we start to see larger deviations because of the different EoS models. In the laboratories on Earth, we can probe the matter somewhere close to $10^{14}\,\mathrm{g\,cm^{-3}}$, after which the densities become too great for us to manipulate.[*] On the other hand, it is exactly starting from this density range that the bulk of the neutron star just starts. Another curious quirk of Nature is how all of the complicated microphysics gets reduced to simple line segments in the logarithmic scales, also known as polytropic pressure relations. In the following sections, we will focus on deriving these simple relations as it helps us in understanding the underlying physics.

2.2 Atmosphere

Atmosphere of a star is the first and uppermost layer responsible for the emergent radiation. Usually, it consists of a thin layer of plasma and ranges from a few millimeters to a couple of centimeters in height, but in some cases if the emerging radiation field is strong enough it can momentarily expand the atmosphere up to

---

[*]Maximum densities reached in the Earth are usually obtained by colliding heavy nucleons together, momentarily creating a core of even denser matter. The densest naturally occurring element found on top of planet Earth is osmium that has an atomic density of "just" $\rho \approx 2.2 \times 10^1\,\mathrm{g\,cm^{-3}}$.
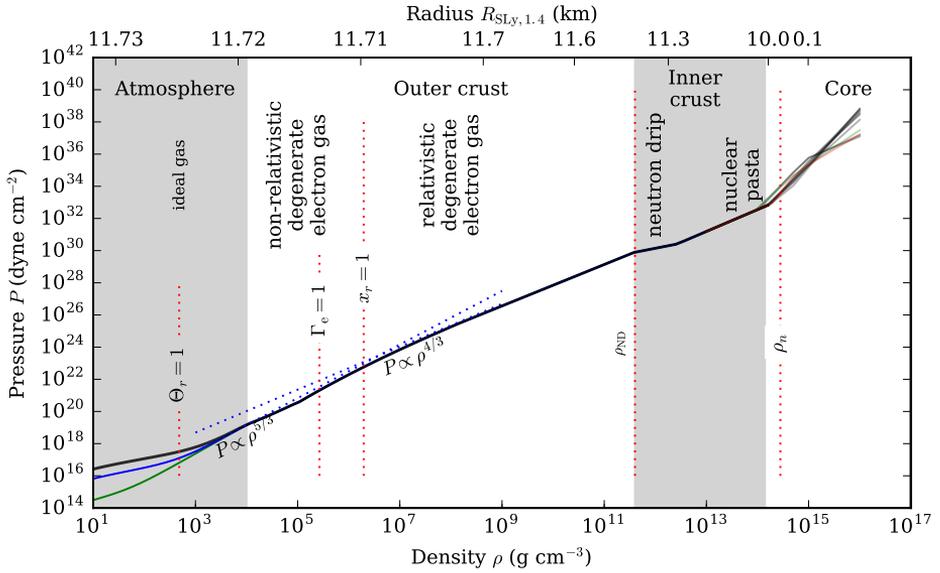
Figure 2.2: Overview of the pressure versus density relation for the full range of densities relevant for neutron stars. Here the evolution of the pressure is shown against the densities depicted in the bottom vertical axis. Green solid line shows the EoS for matter at $T = 10^6$ K, whereas blue line is for $T = 5 \times 10^6$ K, and black for $T = 10^7$ K. Additionally, the upper horizontal axis shows the evolution of the radial coordinate computed for one particular EoS (SLy, see Sect. 2.4) and neutron star configuration (mass of $1.4\,M_\odot$). Different shaded vertical regions show the corresponding interior structures of the star. Additionally, some interesting densities are highlighted with dashed red lines and text labels (see Sects. 2.2−2.4).

several hundreds of meters. In most situations the plasma is in a gaseous state, but in some more rare cases when the magnetic field is extraordinarily strong and the temperature is low, the plasma can condense into a liquid or a solid surface. Such condensed surfaces are, however, rare and usually the gaseous description is more than enough to give an accurate description of the physics of the atmosphere.[62,63]

Properties of the emergent thermal radiation strongly depend on the chemical composition of the atmosphere. In the atmospheres of normal stars, the composition is a mixture of multiple elements. The most stable chemical element on the surface of a neutron star is iron. However, even a small accreted mass of $10^{-17}\,M_\odot$, originating from the surrounding interstellar medium or a binary companion, is enough to cover the whole star, and then a variety of elements are also expected in the neutron star atmospheres. On the other hand, the enormous gravity results in an effective separation of elements leading to a strong sedimentation of the atmosphere where the lighter elements are expected to lay on top of the heavier ones, if the accretion does not constantly replenish the surface layers.[64]

2.2.1 General relativistic effects

The effects from the gravity can be quantified by considering a so-called compactness parameter

$$u = \frac{R_S}{R}, \tag{2.1}$$

where R is the radius of the neutron star and the corresponding Schwarzschild radius is defined as

$$R_S = \frac{2GM}{c^2} \approx 2.95 \frac{M}{M_\odot} \text{ km}, \tag{2.2}$$

where G is the gravitational constant, c is the speed of light, and M is the mass of the star.[65,66] Hence, neutron star has a compactness parameter in the range of $u \approx 1/3$ to $1/2$ resulting in considerable general relativistic corrections. In comparison, the Sun has $u \approx 4.24 \times 10^{-6}$. The compactness is also directly related to the gravitational redshift as

$$1 + z = (1 - u)^{-1/2}, \tag{2.3}$$

that describes how an energy of a photon changes when it has to climb up the gravitational potential well that is created by the star, for example.

Gravitational acceleration under general relativistic theory is

$$g = \frac{GM}{R^2} \frac{1}{\sqrt{1-u}} = 1.38 \times 10^{14} \frac{1}{\sqrt{1-u}} \left(\frac{M}{M_\odot}\right) \left(\frac{10\,\text{km}}{R}\right)^2 \text{ cm s}^{-2}. \tag{2.4}$$

Hence, a surface gravitational acceleration g of $\sim 10^{14}$ to $\sim 10^{15}$ cm s^{-2} is expected for neutron stars. By considering an isothermal atmosphere we can also estimate the scale height as

$$H_a = \frac{k_B T}{m_i g} \approx \frac{0.83}{A} \left(\frac{T}{10^6\,\text{K}}\right) \left(\frac{10^{14}\,\text{cm s}^{-2}}{g}\right) \text{ cm} \tag{2.5}$$

where $k_B = 1.38 \times 10^{-16}$ erg K^{-1} is the Boltzmann constant, T is the temperature of the atmosphere, $m_i = A m_u$, and $m_u \approx 1.66 \times 10^{-24}$ g is the atomic mass unit. From here, the typical scale height values of ~ 1 cm to ~ 10 cm are obtained for atmospheres of $T = 10^6$ and 10^7 K.[62,63] The strong gravitational field also bends the photon trajectories.[67] Hence, in addition to the radius R of the star as measured in the local reference frame, another *apparent* radius, as measured by an observer at infinity,

$$R_\infty = \frac{R}{\sqrt{1-u}}, \tag{2.6}$$

is usually needed when describing the observable features of the atmosphere. From here it is then clear that the atmosphere and the emerging radiation encodes information from the physical parameters of the star. More specifically information about the temperature, surface gravity, chemical composition, and compactness can be obtained.

2.2.2 Radiative transport in the atmosphere

The standard approach in describing the atmosphere structure includes solving three main equations of radiative transfer, hydrostatic balance, and energy conservation. First such a low-B field model of hot neutron star atmospheres were presented in the pioneering work by London et al.[68,69] and Lapidus et al.[70]. Let us next walk through these equations, as they are rather simple. A more general description for the atmosphere model computations are given in[71,72], where the fully relativistic electron scattering is also taken into account, whereas here we only consider the classical elastic (Thomson) scattering.

Because the thickness of the atmosphere is much smaller than the radius of the star,* the atmosphere can be considered in plane-parallel approximation. Rather high densities, on the other hand, allow to consider the plasma of the atmosphere in local thermodynamical equilibrium.

Spectrum, beaming and polarization of emerging radiation can be determined from radiation transfer problem in atmospheric layers. Radiation can be understood as an energy flow, i.e., energy dE per area dA, time dt, frequency interval $d\nu$, and solid angle $d\Omega$. This is known as the specific spectral intensity which we can mathematically formulate as

$$I_\nu = \frac{dE}{dA\, dt\, d\nu\, d\Omega}. \tag{2.7}$$

Radiation averaged over the solid angle, or the so-called mean specific intensity (zeroth moment of I_ν) is then

$$J_\nu = \frac{1}{4\pi} \int_\Omega I_\nu d\Omega = \frac{1}{4\pi} \int_0^{2\pi} d\phi \int_0^\pi I_\nu \sin\theta d\theta = \frac{1}{2} \int_{-1}^{+1} I_\nu d\mu, \tag{2.8}$$

where we have assumed that the radiation does not depend on the azimuthal ϕ angle (as is typical for atmosphere calculations) and introduced $\mu \equiv \cos\theta$ as the cosine of the zenith angle. Net rate of energy flowing across a unit area (for example a photon detector) from *all directions* per time and frequency is known as physical flux.† It is proportional to the first-order moment of I_ν and is defined as

$$F_\nu = 2\pi \int_{-1}^{+1} I_\nu \mu d\mu. \tag{2.9}$$

Similarly, the second-order moment of I_ν, or a so-called K-integral, is

$$K_\nu = \frac{1}{2} \int_{-1}^{+1} I_\nu \mu^2 d\mu, \tag{2.10}$$

which is related to the radiation pressure, as we later on will see.

---

*Recall the scale height of 1 to $10\,\mathrm{cm}$ in comparison to the radius of $10^6\,\mathrm{cm}$.

†Strictly speaking, the first-order moment of I_ν is known as the Eddington flux $H_\nu = \frac{1}{2} \int_{-1}^{+1} I_\nu \mu d\mu$. Physical flux is related to it as $F_\nu = 4\pi H_\nu$ and sometimes one also encounters the "astrophysical" flux defined as F_ν/π.

Now we can introduce the radiative transfer equation for I_ν as

$$\mu \frac{dI_\nu}{d\tau} = \frac{\mu}{\kappa_\nu} \frac{dI_\nu}{dy} = -\frac{\mu}{\rho \kappa_\nu} \frac{dI_\nu}{dz} = I_\nu - S_\nu \tag{2.11}$$

where τ is the optical depth, y is the column density (mass per area), z is the vertical distance from the surface, $\kappa_\nu = \alpha_\nu + \sigma_\nu$ is the total radiative opacity including contributions from the "true" opacity α_ν and from the scattering opacity σ_ν. Here the connection between different independent variables is given as

$$d\tau = \kappa_\nu dy = -\kappa_\nu \rho dz, \tag{2.12}$$

relating the optical depth (distance as experienced by the radiation), column density (projected number density of matter along the path of the radiation), and the height. In addition, we need the source function

$$S_\nu = (\sigma_\nu J_\nu + \alpha B_\nu)\kappa_\nu^{-1}, \tag{2.13}$$

where the scattering term is proportional to the mean spectral intensity J_ν and the "true" absorption term to the thermal Planck function

$$B_\nu(T) = \frac{2h\nu^3}{c^2} \frac{1}{\exp\left[h\nu/(k_B T)\right] - 1}, \tag{2.14}$$

where $h = 6.63 \times 10^{-27}$ erg s is the Planck constant. As a boundary condition for this equation, we can use $I_\nu = 0$ for $\mu < 0$ at $y = 0$ (i.e., the surface). The atmospheres are also usually considered to be in radiative and hydrostatic equilibrium, i.e., (quasi-)stationary. The first requirement assumes that energy is transported by radiation only, i.e., we neglect, for example, conduction and convection. The energy balance in the atmosphere can then be expressed via the radiation flux F only as

$$\int_0^\infty d\nu \int_0^{2\pi} d\phi \int_{-1}^{+1} I_\nu \mu d\mu = F = \sigma_{SB} T_{\text{eff}}^4, \tag{2.15}$$

where $\sigma_{SB} = 5.67 \times 10^{-5}$ erg cm^{-2} s^{-1} K^{-4} is the Stefan-Boltzmann constant, and T_{eff} is the effective temperature. The second requirement of hydrostatic equilibrium, demands that

$$\frac{dP_g}{dy} = g - g_{\text{rad}}, \tag{2.16}$$

where, in addition to the gravitational acceleration g we need the opposing radiative acceleration g_{rad}. Finally, we need to supplement these equations with an equation connecting the gas pressure P_g and density. For the rarefied atmosphere, the ideal gas law is an excellent approximation

$$P_g = nk_B T, \tag{2.17}$$

where n is the number density of particles.

2.2.3 Eddington limit

Usually the atmospheres we calculate are dynamically stable and in hydrostatic balance because large gravity implies $g_{rad} \ll g$. Sometimes, however, the radiation flux might increase to such a strength that it is able to compete against even the enormous gravity of a neutron star. An important limit can then be defined for $g_{rad} = g$, known as the Eddington limit after a renowned astrophysicist Sir Arthur Eddington. Let us now for completeness derive this limit.[73,74]

We can start by formulating an expression for the radiation pressure. This can be easily done when we realize that pressure is just flow of momentum through a surface per unit time and photons carry a momentum of $E/c = h\nu/c$, i.e., projection of the radiation flux into the surface that is considered. In terms of I_ν this is then

$$P_{rad,\nu} = \frac{1}{c} \int_0^{2\pi} d\phi \int_{-1}^{+1} I_\nu \mu^2 d\mu = \frac{4\pi}{c} K_\nu, \qquad (2.18)$$

relating the pressure and the second-order moment K_ν together. Radiative acceleration is then

$$g_{rad} = \frac{dP_{rad}}{dy} = \frac{d}{dy} \int_0^\infty P_{rad,\nu}\, d\nu = \frac{4\pi}{c} \frac{d}{dy} \int_0^\infty K_\nu d\nu. \qquad (2.19)$$

Let us refine this expression by inserting the definition of K_ν and applying the radiative transfer equation (2.11) in the subsequent equation to obtain

$$
\begin{aligned}
g_{rad} &= \frac{4\pi}{c} \frac{d}{dy} \int_0^\infty d\nu \frac{1}{2} \int_{-1}^{+1} I_\nu \mu^2 d\mu \\
&= \frac{2\pi}{c} \int_0^\infty d\nu \int_{-1}^{+1} \mu\, d\mu \left\{ \mu \frac{d}{dy} I_\nu \right\} \\
&= \frac{2\pi}{c} \int_0^\infty d\nu \int_{-1}^{+1} \mu\, d\mu \left\{ \kappa_\nu I_\nu - \kappa_\nu S_\nu \right\}.
\end{aligned}
\qquad (2.20)
$$

We can then simplify equation (2.20) further by assuming isotropic source function $S_\nu(\mu) = S_\nu$ and opacity $\kappa_\nu(\mu) = \kappa_\nu$ to get

$$
\begin{aligned}
g_{rad} &= \frac{2\pi}{c} \int_0^\infty d\nu \int_{-1}^{+1} \mu\, d\mu\, \kappa_\nu I_\nu - \frac{2\pi}{c} \int_0^\infty d\nu \int_{-1}^{+1} \mu\, d\mu\, \kappa_\nu S_\nu \\
&= \frac{2\pi}{c} \int_0^\infty d\nu\, \kappa_\nu \int_{-1}^{+1} I_\nu \mu d\mu + 0 \\
&= \frac{1}{c} \int_0^\infty \kappa_\nu F_\nu d\nu \\
&= \frac{1}{c} \kappa_F F,
\end{aligned}
\qquad (2.21)
$$

where $F = \int_0^\infty F_\nu d\nu$ is the bolometric flux, and

$$\kappa_F = \frac{1}{F} \int_0^\infty \kappa_\nu F_\nu d\nu, \qquad (2.22)$$

is the flux mean opacity.[75,76] From Eq. (2.21) we then see that the radiation acceleration is directly related to the flux of the radiation. Not every photon, however, interacts and collides with the matter, and hence the opacity correction κ_F is also needed. Setting (2.21) equal to g we can solve for the Eddington flux as

$$F_{\mathrm{Edd}} = \frac{gc}{\kappa_F} = \frac{GMc}{R^2 \kappa_F} \frac{1}{\sqrt{1-u}}. \tag{2.23}$$

Usually in many astrophysical scenarios the opacity is dominated by the electron scattering opacity with a characteristic (Thomson) cross-section for the interaction $\sigma_T = 6.65 \times 10^{-25}$ cm^{-2}. Mass for a hydrogen plasma, on the other hand, is mainly set by the protons, hence, opacity per unit mass is then

$$\kappa_F \approx \frac{\sigma_T}{m_p} \approx 0.4\,\mathrm{cm}^2\,\mathrm{g}^{-1}. \tag{2.24}$$

Finally, by calculating the total radiation flux through the stellar surface, we can define a quantity called luminosity as

$$L = 4\pi R^2 F(R), \tag{2.25}$$

where $F(R)$ is the outcoming radiation flux at the surface. Using the aforementioned equation, we can then define the Eddington luminosity for a star as

$$L_{\mathrm{Edd}} = \frac{4\pi GMcm_p}{\sigma_T} \approx 1.3 \times 10^{38} \left(\frac{M}{\mathrm{M}_\odot} \right) \mathrm{erg\,s}^{-1}. \tag{2.26}$$

For neutron stars with surface temperature of $T \sim 10^7$ K this limit can be reached, after which the atmosphere can momentarily expand to counter the excess force as exerted by the radiation.

2.3 Crust

Below the gaseous atmosphere, a solidified layer of matter exists, called crust.[77–79] Between the atmosphere and crust, a liquid ocean of ions also exists, but the interface is not very strict and the matter is smoothly evolving from one state to another. The solidified crust is also typically divided into an outer and inner layer, but the interface is again ambiguous. The pressure here is dominated by the degenerate electrons. In the beginning, the electrons can be taken to be non-relativistic but at about $\rho \sim 10^6$ g cm^{-3} they turn ultra-relativistic because of the increasing density.

By definition, the outer crust is a layer in the neutron star interior where the plasma consists of electrons and nuclei, whereas the inner crust is characterized by an additional appearance of neutrons that start to drip out from the extremely neutron-rich nuclei. The density this occurs is called the neutron drip density and is around $\rho_{\mathrm{ND}} \sim 4 \times 10^{11}$ g cm^{-3}. The outer crust, when defined to begin from the atmosphere at $\rho \sim 10^3$ g cm^{-3} and continue to about ρ_{ND} is only about some hundred meters thick. The characteristics of the matter are strongly dependent on the Coulomb interactions of charged particles that form a solid Coulomb crystal.

The inner crust is taken to continue all the way down to the crust-core interface, where the matter turns liquid again. This layer is about one kilometer thick. Here, at the bottom of the crust, the density is already close to the nuclear density of $\rho_n = 2.8 \times 10^{14}\,\mathrm{g\,cm^{-3}}$ but the exact location of the transition depends on the detailed microphysics of the core. The fraction of free neutrons grows with the increasing density. Because the normal nuclei here are immersed into free neutron gas, the nuclear interactions play a crucial role in defining the matter. Finally, the nuclei disappear totally when we enter the core. Before that, however, the nuclei form complicated structures that evolve together with the density. This region is also known as the nuclear pasta phase, as the different structures are named after the pasta types that they resemble.[80]

2.3.1 Fermi gases

The matter in the crust is degenerate.[81] Let us discuss the physics behind degenerate matter and the related important concept of Fermi energy now. Elementary 6-dimensional phase space cell of any particle is bounded by the Heisenberg uncertainty principle as

$$\Delta x \Delta y \Delta z \Delta p_x \Delta p_y \Delta p_z = h^3, \tag{2.27}$$

where $\Delta x \Delta y \Delta z$ is the volume in ordinary space, $\Delta p_x \Delta p_y \Delta p_z$ the volume in the momentum space, and h is the previously defined Planck constant. In general the number density is given as

$$n_{av} = \frac{g}{\exp[(E - \mu)/k_B T] \pm 1}, \tag{2.28}$$

where + is used for fermions (such as electrons and protons), and − for bosons (such as photons). Additionally, the g is the number of different quantum states a particle may have inside the cell, E is the total particle energy, and μ is the chemical potential that describes the free energy content of the system per particle. Number of particles per unit volume with momentum between p and $p + dp$ is

$$n(p)dp = n_{av} \frac{4\pi p^2}{h^3} dp, \tag{2.29}$$

i.e., particles inside a spherical shell with a surface $4\pi p^2$ and thickness dp. Number density of particles with all momenta is then

$$n = \int_0^\infty n(p)dp. \tag{2.30}$$

The energy in equation (2.28) is the total energy $E \equiv E_{tot} = E_0 + E_k$, composed of the rest-mass energy $E_0 = mc^2$ and kinetic energy E_k. In special relativity, there exists a relation for the total energy as $E_{tot}^2 = (mc^2)^2 + (pc)^2$, so

$$E = mc^2 \left[1 + \left(\frac{p}{mc}\right)^2\right]^{1/2}, \tag{2.31}$$

and the kinetic energy is then simply

$$E_k = mc^2 \left[\left(1 + \left(\frac{p}{mc} \right)^2 \right)^{1/2} - 1 \right]. \tag{2.32}$$

Simple asymptotic limits can be obtained for the kinetic energy as

$$E_k \approx \begin{cases} \dfrac{p^2}{2m} & \text{if } p \ll mc \text{ (non-relativistic)} \\ pc & \text{if } p \gg mc \text{ (ultra-relativistic).} \end{cases} \tag{2.33}$$

Let us now focus on fermions only and select the +-sign (Fermi-Dirac distribution) in Eq. (2.28). Fermions are characterized as spin-$\frac{1}{2}$ particles. In accordance with the quantum mechanics, there is room for only one fermion inside an elementary cell (2.27). The degeneracy parameter g is then equal to 2 because we can have particles of spin $-\frac{1}{2}$ and $+\frac{1}{2}$ in the same "physical location" ($\Delta x \Delta y \Delta z$), as they still have different "momentum locations" ($\Delta p_x \Delta p_y \Delta p_z$) in phase space because of the non-equal spins.

The chemical potential μ in Eq. (2.28) can be expressed as

$$\mu = \epsilon_F + (E - E_k), \tag{2.34}$$

where ϵ_F is a reference energy level known as the Fermi energy. This reflects how the chemical potential is equal to the amount of energy that can be liberated from the system. This is also known as chemical energy. Hence, the number density of fermions in general is

$$n_f = \frac{8\pi}{h^3} \int_0^\infty \frac{p^2 dp}{\exp(\frac{E_k - \epsilon_F}{k_B T}) + 1}. \tag{2.35}$$

If the Fermi energy $\epsilon_F \ll k_B T$, the distribution will be Maxwellian even for small kinetic energies. On the other hand, if $\epsilon_F \gg k_B T$ we can divide the integrand of Eq. (2.35) into two distinct regions of

$$\frac{p^2}{\exp(\frac{E_k - \epsilon_F}{k_B T}) + 1} \approx \begin{cases} p^2 & \text{if } E_k \ll \epsilon_F \\ 0 & \text{if } E_k \gg \epsilon_F, \end{cases} \tag{2.36}$$

with a sharp transition in between at $E_k \approx \epsilon_F$. This allows us to define a characteristic momentum related to the transition energy ϵ_F, called Fermi momentum p_F, so that

$$n_f \approx \frac{8\pi}{h^3} \int_0^{p_F} p^2 dp = \frac{8\pi}{3} \left(\frac{p_F}{h} \right)^3. \tag{2.37}$$

Physically this can be interpreted such that when the temperature decreases, the fermions start to occupy all the quantum states starting from the one with the lowest energy all the way up to the Fermi energy. Because of the Pauli exclusion principle, no more than one fermion can exist in the same quantum state so the levels are

filled in order, and all the higher states will remain empty. Hence, the highest momenta possible in the fully degenerate matter is the Fermi momentum given as

$$p_F = \left(\frac{3n_f}{8\pi}\right)^{1/3} h. \tag{2.38}$$

It is, of course, also related to the Fermi energy simply as

$$\epsilon_F = \frac{1}{2}\frac{p_F^2}{m}, \tag{2.39}$$

that we previously defined merely as a reference energy level. However, from this, the physical interpretation should also become clear as Fermi energy corresponds to the energy of the highest quantum state occupied in the system when temperature reaches zero.

2.3.2 Why neutrons then?

Let us first consider an ideal gas of degenerate electron-proton-neutron plasma to understand the basic composition of the crust.[82] In a degenerate plasma all the quantum states are filled up all the way to the Fermi energy, as we just learned. The normal beta-decay mode for the neutrons, on the other hand, is

$$n \rightarrow p + e^- + \bar{\nu}_e, \tag{2.40}$$

that describes the possible path of how a neutron n will decay into a proton p, electron e^-, and electron antineutrino $\bar{\nu}_e$. It is because of this decay, that we do not expect to see any free neutrons flying around. Such a natural decay, however, might be blocked because there is no room for an emission of an extra electron e^- or a proton p.

Let us then only focus on the decay of the most energetic neutrons with an energy equal to the Fermi energy $\epsilon_F(n)$, where the related particle species is now defined inside the parentheses for clarity. Co-existence of neutrons, protons, and electrons is guaranteed (at zero temperature) if

$$\epsilon_F(n) = \epsilon_F(p) + \epsilon_F(e^-). \tag{2.41}$$

Massive neutrons and protons are to a good approximation non-relativistic up to densities of $10^{14}\,\mathrm{g\,cm^{-3}}$, and hence energy is simply a sum of their rest mass energy and kinetic energy

$$\epsilon_F(n) \approx m_n c^2 + \frac{p_F(n)^2}{2m_n}, \tag{2.42}$$

and

$$\epsilon_F(p) \approx m_p c^2 + \frac{p_F(p)^2}{2m_p}. \tag{2.43}$$

Electrons, on the other hand, are already ultra-relativistic, and so

$$\epsilon_F(e^-) \approx p_F(e^-)c. \tag{2.44}$$

Also note that $n_p = n_e$, as the star is electrically neutral.

From this we can solve $n_n/n_p \sim 5$, 100, and 1000 for $\rho \sim 10^8$, 10^9, and 10^{10} g cm^{-3}, respectively, by taking into account the rest mass difference $m_n - m_p \approx 1.3$ MeV c^2. Thus, we conclude that the matter inside is expected to be neutron rich, even though normally the neutrons would β-decay back to protons and electrons. Not only is the degeneracy then responsible for the pressure but it is also the source of the neutron enrichment.

2.3.3 Degenerate electron gas

Let us next consider the equation of state for the crust. As we have seen, the pressure in the crust originates from the degenerate electron gas. The physics behind this are quite simple, and we repeat the calculations here to introduce the reader to the topic. The result also bears some historical value as these are the equations that were first introduced by Dirac[7], Fowler[8], Frenkel[13], Anderson[10], Stoner[9], and Chandrasekhar[11].[77,81,83–89]

The behavior of the matter in the crust is dominated mainly by the electrons. For this reason, it can be characterized by the electron number density n_e and temperature T_e, hereafter just T in this section. Instead of n_e, let us use the electron Fermi momentum p_F (2.38) as a measure of the number density. It is convenient to describe it in the units of electron rest mass, as

$$x_r \equiv \frac{p_F}{m_e c},$$
(2.45)

also known as the relativity parameter.[85] We will also need the more generic special relativistic form of the Fermi energy

$$\epsilon_F = c \sqrt{(m_e c)^2 + p_F^2},$$
(2.46)

that for a strongly degenerate gas, has the meaning of the chemical potential μ. Finally, the electron Fermi temperature is

$$T_F = \frac{m_e c^2}{k_B} \left(\sqrt{1 + \left(\frac{p_F}{m_e c}\right)^2} - 1 \right) = T_r(\gamma_r - 1),$$
(2.47)

where a typical temperature is

$$T_r = \frac{m_e c^2}{k_B} \sim 6 \times 10^9 \text{ K},$$
(2.48)

and a relativistic scaling factor is defined as

$$\gamma_r \equiv \sqrt{1 + x_r^2}.$$
(2.49)

Then, the temperature can also be expressed in units of T_r as

$$t_r \equiv \frac{T}{T_r}.$$
(2.50)

Using these definitions, it is easy to characterize how relativistic the electron gas is. We can divide it into three regions of

- non-relativistic, for which $t_r \ll 1$ and/or $x_r \ll 1$,

- mildly-relativistic, $t_r \sim 1$ and/or $x_r \sim 1$,

- ultra-relativistic, $t_r \gg 1$ and/or $x_r \gg 1$.

Similarly, we can scale the temperature with the Fermi temperature to get a so-called degeneracy parameter

$$\Theta_F \equiv \frac{T}{T_F}. \tag{2.51}$$

It can be then used to characterize the degeneracy of the plasma to regions of

- non-degenerate, for which $\Theta_F \gg 1$,

- mildly degenerate, $\Theta_F \sim 1$,

- and strongly degenerate, $\Theta_F \ll 1$.

Moving on from an ideal gaseous plasma in the atmosphere, we can start by introducing corrections produced by the closely packed charged particles. In practice, we use the so-called ion-sphere model to describe our Coulomb liquid of ions. We now assume that our ions are emerged into a sea of rigid electron background that takes care of the charge neutrality. In order to couple the number density of electrons and the mass of the plasma, let us first define the mean charge per mass ratio of the plasma as

$$\mu_{Z,A} = \frac{\langle Z \rangle}{\langle A \rangle}, \tag{2.52}$$

where $\langle Z \rangle$ is the mean charge number of the atomic nuclei (for a one-component plasma it is simply Z), and $\langle A \rangle$ is the average number of nucleons bound by one nucleus. For most plasmas, $\mu_{Z,A} \approx \frac{1}{2}$.

Let us now begin by defining a so-called electron sphere radius as

$$r_e = \left(\frac{4\pi n_e}{3} \right)^{-1/3}. \tag{2.53}$$

We can also parameterize the strength between Coulomb (charge) interactions by considering a ratio of potential energy to the kinetic energy with

$$\Gamma_e = \frac{e^2}{r_e k_B T} \approx 22.75 \left(\frac{10^6 \, \text{K}}{T} \right) \left(\frac{\rho}{10^6 \, \text{g cm}^{-3}} \right)^{1/3} \mu_{Z,A}^{1/3}, \tag{2.54}$$

where $e = 4.80 \times 10^{-10}$ esu is the electron charge. Similarly, for ion with a charge number of Z_i, we can define the ion-sphere radius

$$r_i = r_e Z_i^{1/3}, \tag{2.55}$$

that encapsulates enough volume to be charge neutral, when considering the static electron-induced background from n_e. Ion Coulomb coupling factor is similarly

$$\Gamma_i = \Gamma_e Z_i^{5/3} = \frac{(Z_i e)^2}{r_i k_B T}. \tag{2.56}$$

At high temperatures, the electrons form a classical Boltzmann gas. When the temperature is decreased, the plasma will then become a strongly coupled Coulomb liquid corresponding to the neutron star ocean. If the temperature is decreased further, the plasma will transform into a Coulomb crystal. The gaseous regime can be constrained to be at $\Gamma_i \ll 1$, or $T \gg T_B$, where the T_B is given as

$$T_B = \frac{Z^2 e^2}{a_i k_B} \approx 2.28 \times 10^7 \left(\frac{\rho}{10^6 \text{ g cm}^{-3}} \right)^{1/3} \mu_{Z,A}^{1/3} \text{ K}. \tag{2.57}$$

The pressure for such a system can be obtained via the standard thermodynamical relation

$$P = \left(\frac{\partial F}{\partial V} \right)_T, \tag{2.58}$$

where F is the Helmholtz free energy and V is the volume of the system.[81] It is useful to divide the free energy into an ideal part F_{id} corresponding to non-interacting particles, and to the excess part F_{ex}, leading to

$$F(V, T) = F_{id} + F_{ex}. \tag{2.59}$$

Similarly, we could decompose the ideal effects from ions to $F_{id}^{(i)}$ and from electrons to $F_{id}^{(e)}$, yielding

$$F(V, T) = F_{id}^{(i)} + F_{id}^{(e)} + F_{ex}. \tag{2.60}$$

Most important non-ideal deviation for the plasma is from the Coulomb interaction between ions and electrons, and between electrons in the rigid background $F_{ex} \approx F_{ii}$. This free energy decomposition then induces similar division for the pressure

$$P \approx P_{id}^{(i)} + P_{id}^{(e)} + P_{ii}. \tag{2.61}$$

The main contributor for the pressure is the electron degeneracy pressure, $P_{id}^{(e)}$. Other terms, given as $|P_{part}|/P_{id}^{(e)}$, result in leading order terms of[89]

$$\frac{P_{id}^{(i)}}{P_{id}^{(e)}} \approx \frac{\Theta_r^{(i)}}{Z} \tag{2.62}$$

$$\frac{P_{ii}}{P_{id}^{(e)}} \approx \alpha_f \frac{\gamma_r}{x_r}, \tag{2.63}$$

where $\Theta_r^{(i)}$ is the temperature in units of nucleon Fermi temperature (see Eq. 2.51), $\alpha_f = e^2/\hbar c \approx 1/137$ is the fine-structure constant, and $\hbar = h/2\pi$. From here it is

easy to see that only the Coulomb interaction term P_{ii}, should give a measurable correction to the pressure at low temperatures because for the conditions inside neutron stars $\Theta_r^{(i)}$ is very small. This suggests that for the pressure P we can use the approximation

$$P \approx P_{id}^{(e)} + P_{ii}. \tag{2.64}$$

In the weak-coupling limit ($\Gamma_i \ll 1$) the Debye-Hückel result for the excess free energy is a sufficiently good approximation, expressed as[81,90–92]*

$$\frac{F_{ex}}{V} = \frac{1}{\sqrt{3}} n_i kT \Gamma_i^{3/2}, \tag{2.65}$$

where n_i is the ion number density. Hence, the pressure correction due to the Coulomb interactions can be simply presented as

$$P_{ii} \approx -0.3 n_i \frac{Z^2 e^2}{r_i} \tag{2.66}$$

by using Eq. (2.58). Note also that $\Gamma_i = \Gamma_i(V)$ when taking the derivative in respect to the volume when deriving the expression for the pressure.

Let us, as a final task, look into the main degenerate electron pressure term $P_{id}^{(e)}$. Pressure is defined as a flux of momentum through a surface, hence for one particular wall it is

$$P = \int_0^\infty \langle v_x p_x \rangle n(p) dp, \tag{2.67}$$

where the number density $n(p)$ is desribed by the Fermi-Dirac distribution, given by Eq. (2.28). Velocity can be obtained from the standard expression

$$v = \frac{dE}{dp} = \frac{p}{m_e} \left[1 + \left(\frac{p}{m_e c} \right)^2 \right]^{-1/2}, \tag{2.68}$$

using the energy defined by Eq. (2.31). Here we have already inserted the electron mass $m = m_e = 9.11 \times 10^{-28}$ g into the equations. Hence, in the three-dimensional description the pressure is given as one-third of what we would get when inserting Eqs. (2.28), (2.29), and (2.68) into (2.67):

$$P = \frac{1}{3} \int_0^\infty v(p)\, p\, n(p)\, dp = \frac{8\pi}{3 m_e h^3} \int_0^\infty \frac{p}{\left[1 + \left(\frac{p}{m_e c} \right)^2 \right]^{1/2}} p \frac{p^2}{\exp[(E - \mu)/k_B T] + 1} dp. \tag{2.69}$$

Free energy of the system is then equal to what is left from the chemical potential after subtracting the electron rest-mass energy and the pressure contribution,

$$F = (\mu - m_e c^2) n_e - \frac{8\pi}{3 m_e h^3} \int_0^\infty \frac{p^4 dp}{\left[1 + \left(\frac{p}{m_e c} \right)^2 \right]^{1/2}} \frac{1}{\exp[(E - \mu)/k_B T] + 1}. \tag{2.70}$$

---

*Debye-Hückel approximation relays on the assumption that the charge density surrounding an ion is described by electrostatics (Poisson's equation) and the distribution of the charge around the ion itself by thermal motions of electrons (Boltzmann's equation).

Sommerfield expanding the free energy expression in powers of temperature, i.e., t_r, we finally obtain[89]

$$\frac{F}{V} = \frac{m_e c^2}{\lambda_C^3} \frac{1}{8\pi^2} \left(x_r(1 + 2x_r^2)\gamma_r - \ln(x_r + \gamma_r) - \frac{4\pi^2}{3} t_r^2 x_r \gamma_r \right) + O(t_r^4) \qquad (2.71)$$

from which it is easy to obtain an expression for the degenerate electron pressure by applying Eq. (2.58),

$$P_{id}^{(e)} \approx \frac{P_r}{8\pi^2} \left[x_r \left(\frac{2}{3} x_r^2 - 1 \right)\gamma_r + \ln(x_r + \gamma_r) + \frac{4\pi^2}{9} t_r^2 x_r (\gamma_r + \gamma_r^{-1}) \right], \qquad (2.72)$$

where again a typical pressure is given as

$$P_r = \frac{m_e c^2}{\lambda_C^3} \approx 1.4 \times 10^{25} \, \text{dyn cm}^{-2}, \qquad (2.73)$$

and $\lambda_C = \hbar/m_e c = 3.86 \times 10^{-11}$ cm is the reduced electron Compton wavelength.* Omitting the (small) temperature related term ($\propto t_r^2$) leads to the well-known Chandrasekhar equation of state for a perfect, completely degenerate electron gas.[9,83,93]

In the non-relativistic and ultra-relativistic regimes, we can apply the asymptotic limits of Eq. (2.33). Then, the pressure (2.72) takes a simple polytropic form

$$P_{id}^{(e)} \approx \frac{P_r}{9\pi^2 \gamma_{AD}} x_r^{3\gamma_{AD}}, \qquad (2.74)$$

where the polytropic index is given as $\gamma_{AD} = \frac{5}{3}$ or $\gamma_{AD} = \frac{4}{3}$, for the non-relativistic ($x_r \ll 1$) or the ultra-relativistic ($x_r \gg 1$) electrons, respectively. Recall also that $x_r \propto n_e^{1/3} \propto \rho^{1/3}$. The transition occures at $x_r \approx 1$, corresponding to about $\rho \sim 10^6$ g cm^{-3}.

Finally, as suggested by our analysis given in Eq.(2.62), the ideal degenerate electron gas pressure accompanied with the ion Coulomb correction will give us a rather good approximation for the equation of state as

$$P(x_r) \approx P_{id}^{(e)} + P_{ii} = \frac{P_r}{8\pi^2} \left(x_r(\frac{2}{3} x_r^2 - 1)\gamma_r + \ln(x_r + \gamma_r) \right) - 0.3 n_i \frac{Z^2 e^2}{r_i}, \qquad (2.75)$$

remaining valid in a large density range of $10^4 < \rho < 10^{10}$ g cm^{-3}. Below $\rho < 10^4$ g cm^{-3} the plasma is gaseous and the ideal gas law description (2.17) is better suited in modeling the equation of state. Beyond $\rho > 10^{10}$ g cm^{-3} the densities become so high that nuclear degeneracy pressure and more importantly, the mutual nuclear interactions start to play an important role.

---

*Normal Compton wavelength is simply $\lambda_e = 2\pi \times \lambda_C = h/m_e c = 2.43 \times 10^{-10}$ cm.

2.4 Core

After the relatively well-known crust, a physical no-man's land begins when we enter the core. At about half of the nuclear density, $\rho_n \approx 2.8 \times 10^{14}\,\mathrm{g\,cm^{-3}}$, the nuclei become so neutron-rich that more neutrons will leak out then what is left bounded. Hence, normal atoms can no longer exists, and the matter becomes a uniform plasma of neutrons, protons, and electrons. In the end, we will have a liquid sea of free neutrons with a several per cent admixture of protons and electrons. The neutrons and protons, interacting via the nuclear forces, constitute a strongly interacting Fermi liquid, whereas electrons form an almost ideal Fermi gas. Instead of purely degenerate non-interacting matter, like the electrons in the crust, the nucleons become close enough to interact with each other. When in close contact, the repulsive short-range neutron-neutron interaction introduces a considerable stiffening to the equation of state. Hence, a many-body theory is needed in order to describe the matter in the core. If we take the effective range of strong nuclear forces to be of around $r_{sn} \sim 10^{-13}$ cm, we can easily estimate the order-of-magnitude of the density when they become important by equating the mean distance between nucleons to r_{sn}. In this case we obtain $\rho_{sn} \sim m_n/V = 3 \times 1.66 \times 10^{-24}\,\mathrm{g}/4\pi r_{sn}^3 \sim 4 \times 10^{14}\,\mathrm{g\,cm^{-3}}$, a density range surprisingly close to more sophisticated calculations giving $\rho \sim (1.5 - 2) \times 10^{14}\,\mathrm{g\,cm^{-3}}$.[94]

A density range between $0.5\,\rho_n < \rho < 2\,\rho_n$ (i.e., $(1.4 - 5.6) \times 10^{14}\,\mathrm{g\,cm^{-3}}$) corresponds to the *outer core*. For neutron stars it is already several kilometers thick and constitutes a substantial part of the total mass of the star. The matter consists of so-called *npeµ* composition, referring to neutrons n, protons p, electrons e, and in some models to muons μ. The basic physics of this matter is determined by charge neutrality, β-equilibrium, and many-body nuclear interactions. Beyond $\rho > 2\,\rho_n \approx 5.6 \times 10^{14}\,\mathrm{g\,cm^{-3}}$, we have the *inner core*. Its composition is even more unknown and the results here become heavily model-dependent. This is mainly because, in addition to the many-body forces, the exact particle composition is unclear. In addition to the *npeµ* matter, we might have hyperonization (Σ^-, Λ, or more generally sometimes labeled as H), pion condensation (π), kaon condensation (K), or even a phase-transition to a (pure or partial) quark matter (q). Inner core of a neutron star can be many kilometers thick, and the central densities of the most massive stars can go up to $\rho \approx (10 - 15) \times \rho_n \approx (2.8 - 4.2) \times 10^{15}\,\mathrm{g\,cm^{-3}}$.

2.4.1 Polytropes

Instead of trying to obtain a very uncertain nuclear physics description of the equation of state, let us follow an alternative route. As the strongly degenerate equation of state relevant for neutron stars is mainly just the relation between the pressure and the density, we can try and phenomenologically parameterize this relation in contrast to describing the accurate but complicated microphysics. One such a parameterization is a polytropic presentation of the $P(\rho)$ function defined as

$$P(\rho) = K\rho^\gamma, \qquad (2.76)$$

where γ is a polytropic index and is a measure of the *stiffness* of the matter, and K is just a normalization factor. Instead of settling for only one polytrope (actually called a monotrope then), we can link them together to form a piecewise polytropic description of the equation of state. Such a phenomenological description was pioneer by Read et al.[95] In practice, we can then generalize Eq. (2.76) such that

$$P(\rho) = K_i \rho^{\gamma_i}, \quad \text{for } \rho_{i-1} \leq \rho \leq \rho_i, \tag{2.77}$$

for transition densities $\rho_0 < \rho_1 < \rho_2 < \ldots < \rho_{i-1} < \rho_i < \rho_{i+1}$, and so on.

Note that ρ here is the rest-mass density. The energy density ϵ can be obtained from the first law of thermodynamics as

$$d\frac{\epsilon}{\rho c^2} = -P d\frac{1}{\rho c^2}, \tag{2.78}$$

that has an immediate integral of

$$\frac{\epsilon}{\rho} = (1 + a)c^2 + \frac{K}{\gamma - 1}\rho^{\gamma - 1}, \tag{2.79}$$

where a is a continuity constant. Now

$$\lim_{\rho \to 0} \frac{\epsilon}{\rho c^2} = 1, \tag{2.80}$$

implying $a = 0$ for small densities. For the piecewise description we then have (for $\gamma_i \neq 1$)

$$\epsilon(\rho) = (1 + a_i)\rho c^2 + \frac{K_i}{\gamma_i - 1}\rho^{\gamma_i}, \tag{2.81}$$

where

$$a_i = \frac{\epsilon(\rho_{i-1})}{\rho_{i-1}c^2} - 1 - \frac{1}{c^2}\frac{K_i}{\gamma_i - 1}\rho_{i-1}^{\gamma_i - 1}, \tag{2.82}$$

defines the energy density to be a continuous function.

2.4.2 Library for the equation of state of the core

As noticed by Read et al.[95], in most cases, just three piecewise polytropes are enough to give a faithful description of the accurately calculated equations of states, up to a rms error of about 2% in pressure. Here we consider few (relatively) modern descriptions for the dense matter equation of state and parameterize them with polytropes. We follow the naming convention presented in the previous section and divide the compositions into

- normal nuclear matter ($npe\mu$),

- normal nuclear matter mixed with hyperons ($npe\mu + H$),

- normal nuclear matter together with more exotic particles like pion and kaon condensates ($npe\mu + \pi + K$), and

- matter consisting of (or normal matter mixed with) quarks (q or $npe\mu + q$).

The different equations of states we describe here are commonly used in the literature[96–98] and are fitted with polytropes by Read et al.[95] Additionally, we require that the maximum mass of the equation of state fulfills the $2\,M_\odot$ mass limit as set by astrophysical measurements of binary pulsars.[99–101] For $npe\mu$ composition we include models computed with

- potential method using SLy effective nuclear interaction that is of Skyrme-type,[102]

- four variational method EoSs, APR3/4[103] and WFF1/2,[104]

- two relativistic Brueckner-Hartree-Fock calculations, ENG[105] and MPA1,[106] and

- two relativistic mean-field theory models, MS1 and MS1b (same as MS1 but with lower symmetry energy).[107]

For hyperon models ($npe\mu + H$) we include

- one variant of relativistic mean-field theory model, H4.[98]

Here the introduction of hyperons into the matter considerably softens the equation of state and the stars constructed with these models do not end up reaching the $2\,M_\odot$ limit. Similarly, models where mesons, like pion and kaon condensates ($npe\mu + \pi$ and/or $npe\mu + K$) are taken into account, end up not being stiff enough. Finally, for the hybrid nuclear matter and quark matter compositions ($npe\mu + q$) we include

- mixed APR nuclear matter and color-flavor-locked quark matter EoS ALF2.[108]

Again, for pure quark matter composition, the equation of state ends up being too soft. Even in the case of the ALF2, the transition density from the nuclear matter to quark matter is defined at a relatively late phase corresponding to $\rho = 3\,\rho_\mathrm{n}$.

These 11 equations of states end up giving quite a good overview of different models present in the literature. We, however, stress that by no means is it a complete list. The corresponding $P(\rho)$ evolution of these models is shown in Fig. 2.3. Unlike the previously well-defined crust, here the theoretical uncertainties become obvious as there is quite a large scatter in between different models.

2.5 Tolman-Volkoff-Oppenheimer equations

Let us, as a final task, try and construct an actual model of a star from the equation of state. For this, we require the star to be in hydrostatic equilibrium so that the pressure gradient of the matter opposes the gravity. In classical Newtonian form this can be expressed simply as

$$\frac{dP}{dr} = -\frac{Gm\rho}{r^2},$$
(2.83)
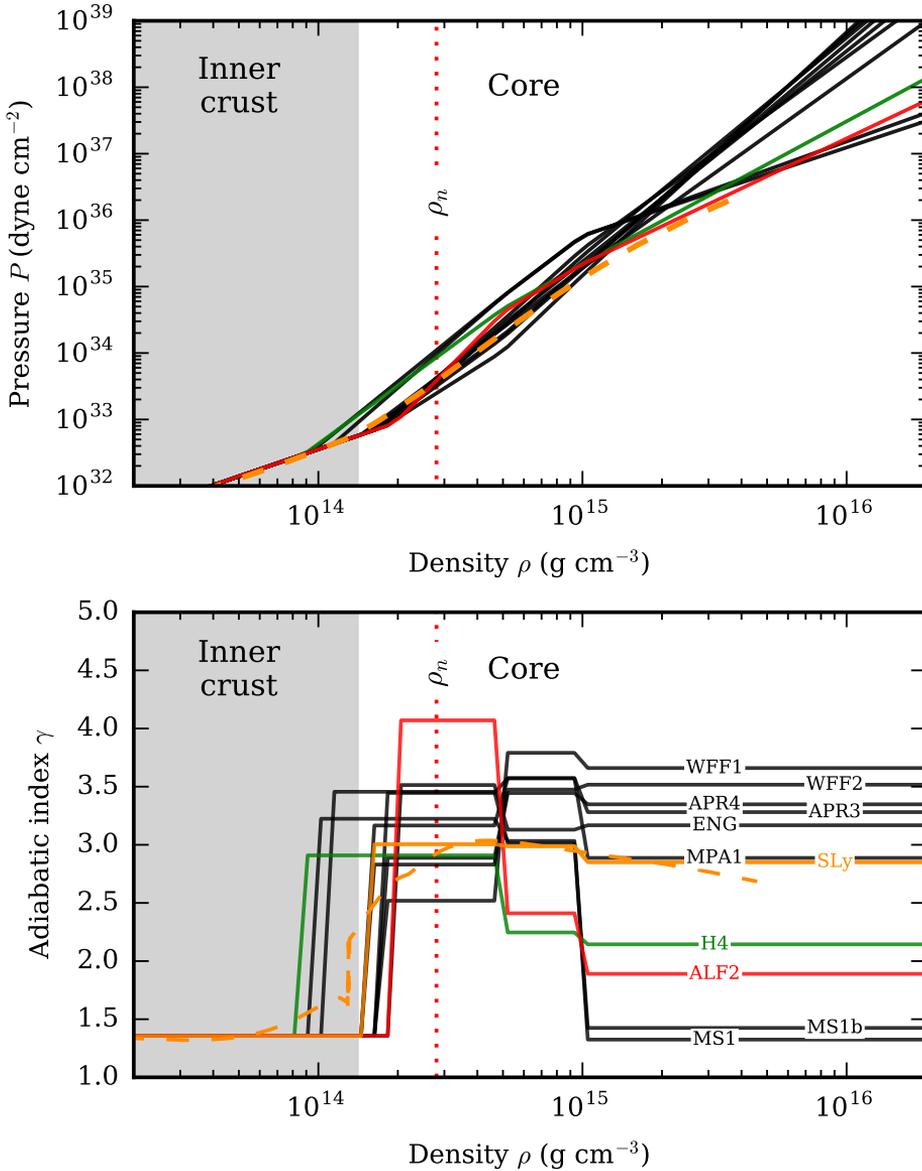
Figure 2.3: Equation of states for the core. *Top:* Pressure versus density relation, $P(\rho)$. *Bottom:* Corresponding adiabatic or the polytropic index evolution versus the density, $\gamma(\rho)$. Plain nuclear matter models are colored in black, hyperonic ($npe\mu + H$) with green, and quark (q) matter in red. Additionally, the exact SLy model (shown exceptionally in dark orange) is shown with dashed lines. Grey region highlights the crust densities and the red dotted vertical line shows the nuclear density of $\rho_n = 2.8 \times 10^{14}\,\mathrm{g\,cm^{-3}}$.

where r is the radial coordinate. In addition, we will need a connection for the mass m and radius r, that in spherical symmetry is given as

$$\frac{dm}{dr} = 4\pi r^2 \rho. \tag{2.84}$$

32

Taking into account the general relativistic corrections we get

$$\frac{dP}{dr} = -\frac{GM\rho}{r^2} \times \frac{(1 + P/\rho c^2)(1 + 4\pi r^3 P/mc^2)}{1 - 2Gm/rc^2}. \tag{2.85}$$

This is the relativistic hydrostatic equilibrium equation as first derived by Tolman[15], Oppenheimer and Volkoff[16]. Difference in respect to the classical formulation originates from the source of gravity: in the Newtonian case it is the mass m, whereas in the general relativity it is the energy momentum tensor that depend both on the energy density and the pressure. As a result, both, energy and pressure, give rise to a gravitational field.

This has an important consequence for the stability of compact stars: Successive increase in the pressure to counter the gravity is ultimately self-defeating. We can get an idea of this, by using an unphysical but analytically easier special case of constant density, i.e. incompressible equation of state, as our model. By solving Eq. (2.83) for constant density $\rho(r) = \rho_0$, we obtain

$$P(r) = G\frac{2\pi}{3}\rho_0^2(R^2 - r^2) \tag{2.86}$$

whereas the general relativistic form described by Eq. (2.85) gives, after some tedious algebra,

$$P(r) = \rho_0 c^2 \frac{\sqrt{1 - u\left(\frac{r}{R}\right)^2} - \sqrt{1 - u}}{3\sqrt{1 - u} - \sqrt{1 - u\left(\frac{r}{R}\right)^2}}, \tag{2.87}$$

where again the compactness parameter $u = 2GM/Rc^2$ is used. Unlike the classical counter-part, the general relativistic central pressure $P(0)$ is undefined for $u \geq u_{\max} = \frac{8}{9}$, which corresponds to

$$M_{\max} = \frac{4}{9}Rc^2/G \approx 3.01\left(\frac{R}{10\,\text{km}}\right)\,\text{M}_\odot. \tag{2.88}$$

Even though the assumption of constant density is unphysical, the solution shows that the relativistic equations of hydrostatic balance have a maximum mass after which the star becomes unstable. This is an important feature of the equations as it can be used, for example, to rule out certain equations of states, given that we have measured some (large) neutron star mass to exist in Nature. It was also the source of confusion in the 1930s because the degenerate neutron gas equation of state gives $M_{\max} \approx 0.7\,\text{M}_\odot$, while the Chandrasekhar limit, i.e., the maximum mass for white dwarfs with degenerate electrons, give $M_{\text{Ch}} \approx 1.44\,\text{M}_\odot$. From these arguments, it would seem that neutron stars can not exist because the maximum mass is less than that of the white dwarfs. Now we, of course, already know that it is the nuclear many-body interactions that have a huge impact on the equations of states and subsequently alter the maximum mass to be of around $M_{\max} \approx (1.5 - 3)\,\text{M}_\odot$. Similarly, the measurements of $M \approx 2.0\,\text{M}_\odot$ neutron stars, that we already
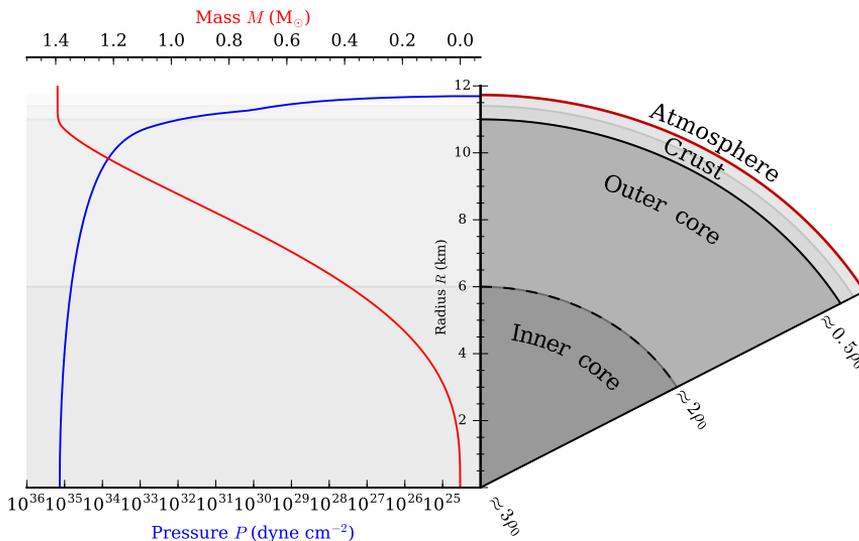
Figure 2.4: Overview of the neutron star structure for the SLy equation of state and core density of $P_{\mathrm{c}} = 8.9 \times 10^{14} \, \mathrm{g\,cm^{-3}}$, corresponding to $M = 1.4 \, \mathrm{M_\odot}$. Right side of the figure shows a schematic presentation of the star's interiors against the radial coordinate, whereas the left side shows the pressure (blue; bottom axis) and cumulative mass (red; top axis) evolution from the core to the surface.

used to rule out some equations of states in the previous section, put stringent constraints on the possible behavior of the matter.

Instead of looking at the different quantities, such as the pressure, as a function of the density, let us now finally solve the structure of the star given the derived equations of states. The results are obtained by numerically solving the Tolman-Oppenheimer-Volkoff equations using the previously presented crust model and the different equations of states for the core.* In Fig. 2.4 the dependency of the pressure and cumulative mass of the star against the radial coordinate (as measured starting from the core) is visualized for the SLy equation of state for a central density of $P_{\mathrm{c}} = 8.9 \times 10^{14} \, \mathrm{g\,cm^{-3}}$, corresponding to $M = 1.4 \, \mathrm{M_\odot}$. This visualizes the real dimensions of the neutron stars internal structure: Inner core spans about 6 km in radius from the center while the outer core extends from 6 to 11 km. The full crust is only about ~1 km thick, and the atmosphere is too thin to be even visible. The core also contains more than 99% of the total mass of the star.

Instead of fixed central pressure, we can let it span a large range, starting from some small value and ending to the pressure corresponding to the maximum mass, to obtain mass−radius, or more succinctly, $M-R$ curves for the equations of states. These are visualized in Fig. 2.5 along with the pressure−density relations that yield them. From here it is obvious how the large uncertainty in the nuclear physics of the core then translates into a large possible allowed radius range, from about 10 to

---

*TOV-solver that is used is available from `https://github.com/natj/tov`.
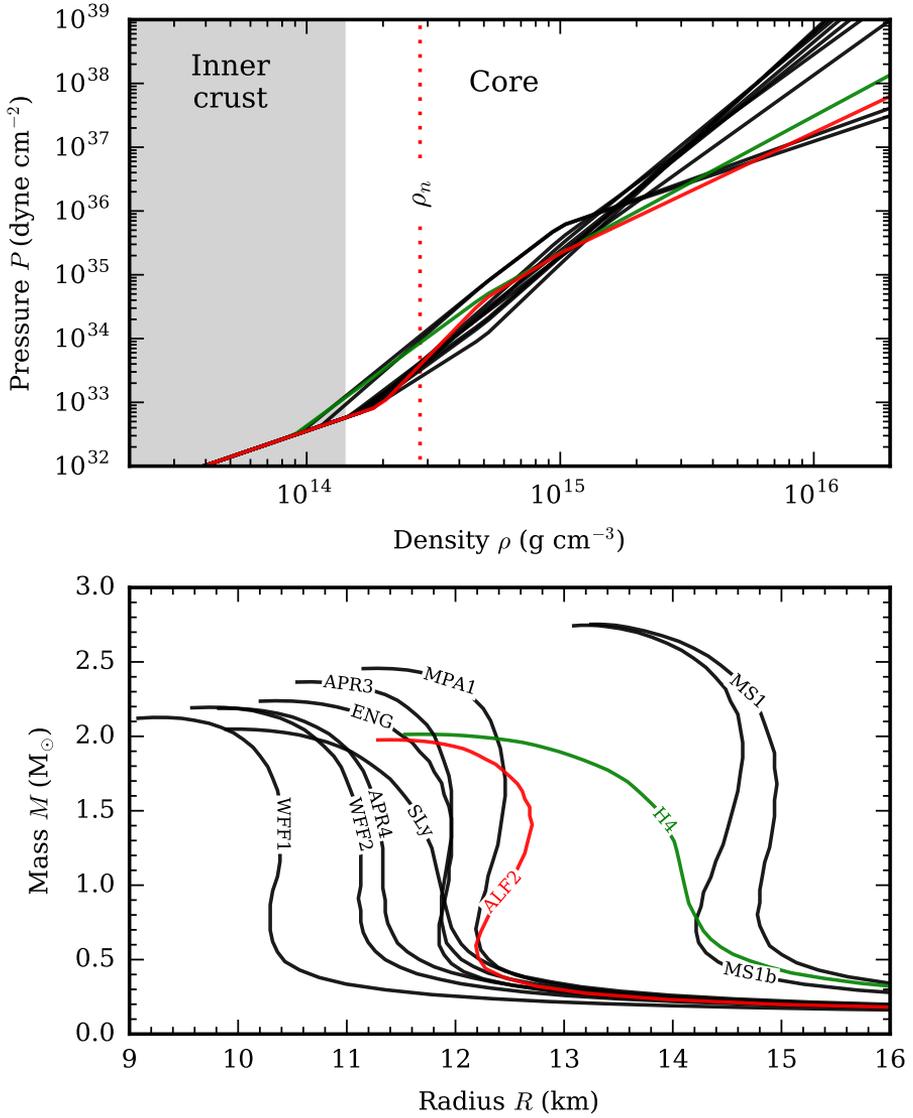
Figure 2.5: Equation of states and the resulting neutron star mass-radius curves for the different core models. *Top:* Pressure versus density relation, $P(\rho)$. *Bottom:* Corresponding $M - R$ relations. Symbols and colors are the same as in Fig. 2.3.

15 km. It also opens up a pathway of probing the nuclear physics with astrophysics because mass and radius measurements of real neutron stars can set constraints on the equation of state.
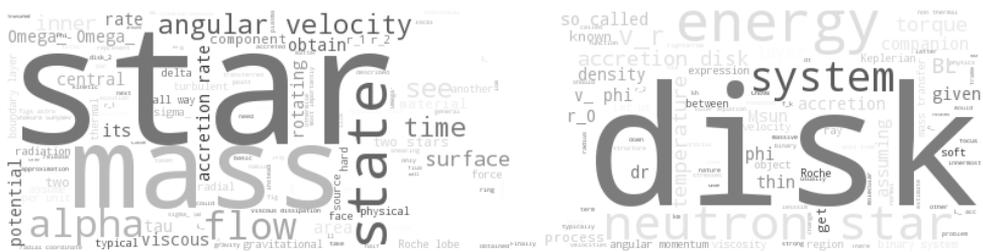
3 | Astrophysics around neutron stars

Let us next discuss the violent environments of neutron stars and the related astrophysics therein. These surroundings also play an important role when we try to decipher different kinds of observations of neutron stars. In the heart of this whole problem is an astrophysical process called accretion. This is a process where matter is transferred from a one star to another because of the gravitational forces. Most importantly, the infalling material has to somehow lose its angular momentum before it is able to travel all the way to the neutron star surface. Nature's platform for this is called an accretion disk. Sometimes the disk also continues all the way to the surface of the neutron star. Instead of smoothly joining the star, this process is often violent and leads to another source of radiation as this so-called boundary layer heats up when the rapidly rotating inner disk tries to slow down to velocities similar to that of the more gently rotating star.

We begin by discussing the basics of the accretion process and present some order-of-magnitude estimates relevant for the accretion disks and boundary layers. Most importantly, we try to characterize the strength of the radiation originating from them.

3.1 Accretion

Accretion is an astrophysical process that has its roots in the gravity. It can be a source of an enormous amount of energy if the central object is compact, because the depth of a gravitational well is directly proportional to the compactness of the central source. Hence, it is an important, and often dominating, process for neutron stars.[74]

Gravitational potential energy release for a mass m that is accreted onto a compact object of a radius R and a mass M is

$$\Delta E_{\text{acc}} = m\frac{GM}{R} \sim 10^{20} \left(\frac{m}{\text{g}}\right)\left(\frac{10\,\text{km}}{R}\right)\left(\frac{M}{\text{M}_\odot}\right) \text{erg}, \qquad (3.1)$$

where in the latter expression typical dimensions of neutron star are used.

This energy, 10^{20} erg per each gram that is accreted, is usually released as radiation. The rate of this energy release is simply related to the mass accreted per unit time, i.e., accretion rate $\dot{M} = \Delta M/\Delta t$,

$$L_{\text{acc}} = \dot{M}\frac{GM}{R} \approx 1.3 \times 10^{36} \left(\frac{\dot{M}}{10^{16}\,\text{g s}^{-1}}\right)\left(\frac{10\,\text{km}}{R}\right)\left(\frac{M}{\text{M}_\odot}\right) \text{erg s}^{-1}, \qquad (3.2)$$

where a typical value of $\dot{M} \sim 10^{16}\,\mathrm{g\,s^{-1}} \approx 1.5 \times 10^{-10}\,\mathrm{M_\odot\,yr^{-1}}$ is taken for the accretion rate. For higher accretion rate, L_{acc} can reach the Eddington luminosity (Eq. (2.26)) of a neutron star.

3.1.1 Roche lobes and mass transfer in binary systems

In order to use the accretion as an energy source, mass transfer needs to take place in the system. For the mass transfer to keep on operating, a source of fresh material is needed. In binary systems with two stars, the companions star is the obvious fuel resource. Here we will focus on the so-called Low Mass X-ray Binary (LMXB) systems where the companion, like the name implies, is a relatively low-mass star with a mass $M \lesssim 1\,\mathrm{M_\odot}$.[109] Such a setup leads to a mass-transfer quite naturally as the heavier neutron star will just rip out the outer layers of its poor companion and starts slowly consuming it. As another option, the system could be a so-called High Mass X-ray Binary (HMXB) system, where the companion of the neutron star has $M \sim 10\,\mathrm{M_\odot}$, and the accretion happens, for example, via a neutron star capturing the strong wind from the companion. Here in this thesis, we will, however, only focus on the LMXB systems.

How exactly is the material transferred from the companion to the primary star is an interesting problem. We can begin to understand the physical setup by considering a general hydrodynamical system of two objects in a rotating frame. Here we select the frame that co-rotates with the binary system. The subsequent flow of gas between the two stars can then be described by the Euler equation with additional Coriolis and centrifugal terms.[110] In practice the Euler equation describes the time evolution of the velocity $\boldsymbol{v}$ of the gas that has a pressure P and density ρ. In a reference frame rotating together with the binary system with angular velocity ω the Euler equation takes the form

$$\frac{\partial \boldsymbol{v}}{\partial t} + (\boldsymbol{v} \cdot \nabla)\boldsymbol{v} = -\nabla \Phi_{\mathrm{R}} - 2\boldsymbol{\omega} \times \boldsymbol{v} - \frac{1}{\rho}\nabla P, \tag{3.3}$$

where the angular velocity of the binary is

$$\omega = \left(\frac{GM}{a^3}\right)^{1/2} \boldsymbol{e}, \tag{3.4}$$

as given with the unit vector $\boldsymbol{e}$ normal to the orbital plane. Here M is the total mass of the system, i.e., $M = M_1 + M_2$, where M_1 and M_2 are the individual masses of the two stars in the system, respectively, and a is their orbital separation.

The effects originating from the gravitation and from the centrifugal forces are encapsulated in the so-called Roche potential, given as a function of radial vector $\boldsymbol{r}$ as[111,112]

$$\Phi_{\mathrm{R}}(\boldsymbol{r}) = -\frac{GM_1}{|\boldsymbol{r} - \boldsymbol{r_1}|} - \frac{GM_2}{|\boldsymbol{r} - \boldsymbol{r_2}|} - \frac{1}{2}(\boldsymbol{\omega} \times \boldsymbol{r})^2, \tag{3.5}$$

where the locations of the stars are given with $\boldsymbol{r_1}$ and $\boldsymbol{r_2}$. By studying the shape of the potential, we see that in between the two stars, in the so-called L_1 point there exists a location where the countering gravitational forces from the two stars are
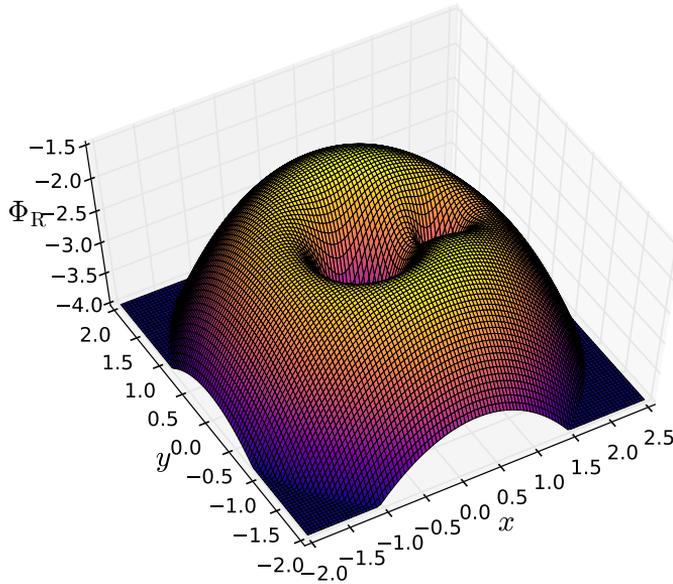
Figure 3.1: Two-dimensional Roche potential $\Phi_R(x, y)$ visualized for a binary system with $M_1/M_2 = 0.25$ and $a = 1$. The nozzle (L_1 point) is visible as a valley (or more specifically, a saddle point) between the gravitational wells of the two stars.

balanced. This can be thought of as a physical nozzle in the system from which the less massive star will leak material into the more massive star. Such a mass transfer, also known as a Roche lobe overflow, will then occur if the companion star's radius exceeds the size of its own individual Roche lobe visualized in Fig. 3.1. Typically, such a thing can happen when the star evolves and expands at the end of its life cycle.

3.1.2 Accretion disks

When the mass transfer has started via the Roche lobe overflow, and we have a stable source of material that is being transferred from the companion to the more massive neutron star, we can next focus on the region where gravitational forces of the neutron star dominate. Originally, we can think of each individual incoming particle having their own circular orbit around the central object. The mass flow, i.e., the stream of particles, is confined into the orbital plane of the binary system, hence, the problem of describing the physics of the flow is one dimensional as a first approximation because only radial coordinate r is considered. This is known as the so-called thin-disk approximation. The nested circular orbits of the plasma can be naturally described in cylindrical coordinates, hence the word "disk". Sec-

ondly, the scale height H of the disk is small compared to the radial coordinate ($H \ll r$), so we say that the disk is thin.

Radial structure of the disk can then be obtained from the Keplerian rotation law as

$$\Omega_K(r) = \left(\frac{GM}{r^3}\right)^{1/2},$$

(3.6)

describing an angular velocity as a function of radial coordinate from the disk center. There is an important detail hidden here in the Kepler's law: Keplerian angular velocity implies differential rotation, i.e., varying angular velocities as a function of r. Such a shearing between two adjacent annuli will then lead to viscous stresses.

The disk's structure can be obtained from the hydrodynamical equations in cylindrical coordinates. Instead of the density ρ, let us use the surface density $\Sigma = 2H\rho$ to describe the mass. Conservation of mass and angular momentum can then be written as[74,110]

$$r\frac{\partial \Sigma}{\partial t} + \frac{\partial}{\partial r}(r\Sigma v_r) = 0,$$

(3.7)

and

$$r\frac{\partial}{\partial t}(\Sigma r^2 \Omega) + \frac{\partial}{\partial r}(r\Sigma v_r r^2 \Omega) = \frac{1}{2\pi}\frac{\partial \tau}{\partial r},$$

(3.8)

where v_r is the velocity in r direction and τ is the viscous torque of the differentially rotating disk.

Torque, in general, can be understood as an angular momentum flux density per unit time and is given by

$$\tau_i = \epsilon_{ijk} r_j f_k,$$

(3.9)

where ϵ_{ijk} is the Levi-Civita symbol, and f_k is the force density, i.e., momentum density flux per unit time, given as

$$f_k = \sigma_{kh} n_h.$$

(3.10)

Here σ_{kh} is the kh-component of a general stress tensor σ_{ij}, and n_h is some surface normal of the area where the shearing takes place. In our case, we can compute the shear in cylindrical coordinate system focusing on r and ϕ coordinates only as[110]

$$\sigma_{r\phi} = \rho v \left(r\frac{\partial}{\partial r}\left\{\frac{v_\phi}{r}\right\} + \frac{1}{r}\frac{dv_r}{d\phi}\right),$$

(3.11)

which simplifies to

$$\sigma_{r\phi} = \rho v r \frac{d\Omega}{dr},$$

(3.12)

when we remember that $v_\phi = r\Omega$ and assume the flow to be symmetric in the azimuthal ϕ-direction ($\partial v_r/\partial \phi = 0$). The total viscous torque acting at the $2\pi r(2H)$ area corresponding to the disk rim at location r is then

$$\tau(r,t) = 2\pi r v \Sigma r^2 \frac{d\Omega}{dr}.$$

(3.13)

Combining the latter expressions and assuming Keplerian rotation $\Omega(r) = \Omega_K(r)$ with a fixed central mass of M (i.e., $\partial\Omega/\partial t = 0$), we can then solve the system of equations and obtain expressions for the surface density and the radial velocity as

$$\frac{\partial\Sigma}{\partial t} = \frac{3}{r}\frac{\partial}{\partial r}\left[r^{1/2}\frac{\partial}{\partial r}(\nu\Sigma r^{1/2})\right], \tag{3.14}$$

and

$$v_r = -\frac{3}{\Sigma r^{1/2}}\frac{\partial}{\partial r}(\nu\Sigma r^{1/2}). \tag{3.15}$$

In order to continue further, we would need a description for the viscosity ν. It could have its roots on the normal molecular viscosity[113] or like the current theories imply, be magnetohydrodynamic in nature. The latter is known as the magnetorotational instability (MRI) where magnetic stresses of turbulent field lines cause viscosity for the plasma.[114–116] As another approach, we should also mention the widely successful α parameterization by Shakura & Sunyaev, known as the "standard disk" or α-disk.[117] This method is mostly mathematical as we just reparameterize our ignorance of the viscosity into a new parameter called α, that is taken to be proportional to the local soundspeed c_s and height of the disk H, as $\nu = \alpha c_s H$. Even though only mathematical in nature, this formulation has turned out to be extremely successful in helping to explain the basic functionality of accretion disks because α can be treated as a small parameter in all the subsequent formulae. The physical reason for the smallness of α is also intuitive: velocities can not be larger than the local soundspeed, otherwise supersonic flows would produce shocks that would dissipate energy until the local velocities are subsonic again. Similarly, the size of the turbulent eddies must be smaller than the disk scale height. Together these then imply $\alpha \lesssim 1$.

To get some idea of the disk dynamics, we can, as our zeroth order approximation assume $\nu = $ constant. Then, the time-dependent disk structure (Eqs. (3.7) and (3.8)) can be solved, for example, by assuming as an initial condition a ring of mass m at $r = r_0$,

$$\Sigma(r, t = 0) = \frac{m}{2\pi r_0}\delta(r - r_0), \tag{3.16}$$

where δ is the Dirac delta function. As a solution, we then obtain a mass distribution that slowly diffuses due to viscosity as

$$\Sigma(\tilde{r}, \tilde{t}) = \frac{m}{\pi r^2}\frac{1}{\tilde{t}\,\tilde{r}^{1/4}}\exp\left[-\frac{(1 + \tilde{r}^2)}{\tilde{t}}\right]I_{1/4}\left(\frac{2\tilde{r}}{\tilde{t}}\right), \tag{3.17}$$

where $I_{1/4}(x)$ is the modified Bessel function, $\tilde{r} \equiv r/r_0$ is the dimensionless radial coordinate, and $\tilde{t} \equiv 12\nu t/r_0^2$ is the dimensionless time. Inserting (3.17) into (3.15), we also obtain

$$v_r(\tilde{r}, \tilde{t}) = -\frac{3\nu}{r_0}\frac{\partial}{\partial\tilde{r}}\left[\frac{1}{4}\ln\tilde{r} - \frac{(1 + \tilde{r}^2)}{\tilde{t}} + \ln I_{1/4}\left(\frac{2\tilde{r}}{\tilde{t}}\right)\right]. \tag{3.18}$$

Which in the asymptotic limits give

$$
v_r \sim
\begin{cases}
\dfrac{3\nu}{r_0}\left(\dfrac{1}{4\tilde{r}} + \dfrac{2\tilde{r}}{\tilde{t}} - \dfrac{2}{\tilde{t}}\right) > 0 & \text{for } 2\tilde{r} \gg \tilde{t} \\[3mm]
-\dfrac{3\nu}{r_0}\left(\dfrac{1}{2\tilde{r}} - \dfrac{2\tilde{r}}{\tilde{t}}\right) < 0 & \text{for } 2\tilde{r} \ll \tilde{t}.
\end{cases}
\tag{3.19}
$$

Even from this simplified treatment we can understand the basic physics of how the accretion disks operate: The viscous shear stresses help the rotating plasma redistribute its angular momentum outwards while at the same time most of the mass is accreted inwards.

Let us next study a steady-state disk solution by setting $\partial/\partial t \to 0$. From the angular momentum conservation (3.8), we obtain

$$
r\Sigma v_r r^2 \Omega = \frac{\tau}{2\pi} + \frac{C}{2\pi},
\tag{3.20}
$$

with a constant C that physically represent a torque term from the coupling of the inner disk and the star at $r \approx R$. In short,[*] it is given by

$$
C \approx -\dot{M}(R)R^2\Omega(R) \approx -\dot{M}R^2\Omega_K(R) = -\dot{M}(GMR)^{1/2},
\tag{3.21}
$$

with the expression for the mass accretion rate given in terms of the radial velocity v_r as

$$
\dot{M}(r) = -\frac{2\pi r\Sigma dr}{dt} = -2\pi r\Sigma v_r,
\tag{3.22}
$$

and assuming a thin layer for the zone where the inner disk angular velocity is slowed down to the angular velocity of the star (otherwise, we could not set $r \to R$). Substituting this into (3.20), and assuming Keplerian angular velocity profile, we obtain

$$
\nu\Sigma = \frac{\dot{M}}{3\pi}\left[1 - \left(\frac{R}{r}\right)^{1/2}\right].
\tag{3.23}
$$

Physically this represents a steady-state solution of a disk with central torque applied to it. Viscous dissipation rate per unit disk face area is then[†]

$$
D(r) = \frac{\tau\Omega'}{4\pi r} = \frac{1}{2}\nu\Sigma(r\Omega')^2 = \frac{3GM\dot{M}}{8\pi r^3}\left[1 - \left(\frac{R}{r}\right)^{1/2}\right].
\tag{3.24}
$$

Finally, from here we can compute the luminosity of the disk faces due to energy lost by viscous dissipation

$$
\begin{aligned}
L(r_1, r_2) &= 2\int_{r_1}^{r_2} D(r)2\pi r\, dr = \frac{3GM\dot{M}}{2}\int_{r_1}^{r_2}\left[1 - \left(\frac{R}{r}\right)^{1/2}\right]\frac{dr}{r^2} \\
&= \frac{3GM\dot{M}}{2}\left\{\frac{1}{r_1}\left[1 - \frac{2}{3}\left(\frac{R}{r_1}\right)^{1/2}\right] - \frac{1}{r_2}\left[1 - \frac{2}{3}\left(\frac{R}{r_2}\right)^{1/2}\right]\right\},
\end{aligned}
\tag{3.25}
$$

---

[*]Torque is alternatively defined via the linear momentum $\boldsymbol{p} = mv_\phi\hat{\boldsymbol{e}}_\phi$, as $\tau = d(\boldsymbol{r} \times \boldsymbol{p})/dt = rv_\phi dm/dt = r^2\Omega\dot{M}$. This again represents the flow of angular momentum in the system.

[†]Viscous dissipation rate in ring of width dr is $\tau\Omega' dr$, i.e., the rate of work done by the torque, and the total area of the ring, taking into account both the lower and upper faces, is $4\pi r dr$. Hence, we obtain Eq. (3.24) as the ratio of these.

and by then setting $r_1 \to R$ and $r_2 \to \infty$, we get

$$L_{\mathrm{disk}} = \frac{GM\dot{M}}{2R} = \frac{1}{2}L_{\mathrm{acc}}. \tag{3.26}$$

Hence, half of the potential energy will be lost by the viscous shearing and is radiated away by the upper and lower faces of the accretion disk. Importantly, the other remaining half will be transferred all the way to the star.

Temperature of the hottest inner disk can be estimated by assuming an optically thick media and using the dissipation rate D as the surface flux. This innermost region of the disk is the brightest because here the gravity is the strongest and the dissipation area the smallest. An estimate for the disk surface temperature can then be obtained from

$$\sigma_{\mathrm{SB}} T_{\mathrm{disk}}^4(r) \sim D(r). \tag{3.27}$$

From here we obtain

$$T_{\mathrm{disk}}(r) = T_* \left[1 - \left(\frac{R}{r} \right)^{1/2} \right]^{1/4} \left(\frac{R}{r} \right)^{3/4}, \tag{3.28}$$

where

$$T_* = \left(\frac{3GM\dot{M}}{8\pi R^3 \sigma_{\mathrm{SB}}} \right)^{1/4} \approx 2.3 \times 10^7 \left(\frac{\dot{M}}{10^{16}\,\mathrm{g\,s^{-1}}} \right)^{1/4} \left(\frac{M}{\mathrm{M_\odot}} \right)^{1/4} \left(\frac{R}{10\,\mathrm{km}} \right)^{-3/4} \mathrm{K}, \tag{3.29}$$

is a typical temperature in the innermost regions of the disk.

Observationally we see that the disks are, however, not as simple as discussed here.[118] The standard α-disk model assumes steady-state, whereas in reality the disk structure evolves in time. Most importantly, the mass accretion rate is seen to vary over long timescales. From observations, we also know that the disks alternates between three states called, quiescent, hard and soft state.[118–123]

The soft (also known as "high" or "thermal-dominant") state is characterized by a strong soft component in the observed spectra.[124] There is, however, also a complex non-thermal tail usually present.[125] Here the soft component could be interpreted as a thermal radiation from an optically thick disk but the non-thermal tail implies that this picture is not complete. The hard (also known as "low") state is even more complicated as the observational spectra is dominated by a strong hard X-ray component but some signs of a low-temperature thermal disk is also sometimes visible.[126] In the final quiescent, or "off" state, the observed flux typically drops below the detection limit and we do not see anything.

The current physical interpretation of these two states can be satisfactorily explained by a truncated disk model with a hot inner flow. Here the disk, well-described by the Shakura & Sunyaev α-disk is truncated, i.e., does not always reach the central object. The cool and optically thick, geometrically thin, disk is then responsible of the low-energy thermal radiation. In the innermost parts, the disk turns into hot, optically thin flow, that is also responsible for the non-thermal

Soft/high state
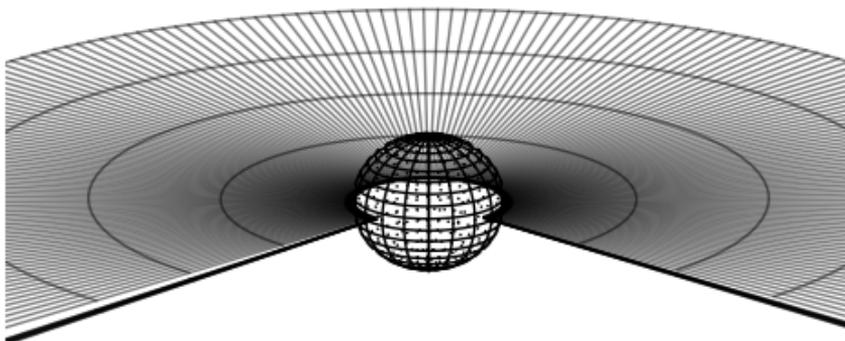
Hard/low state
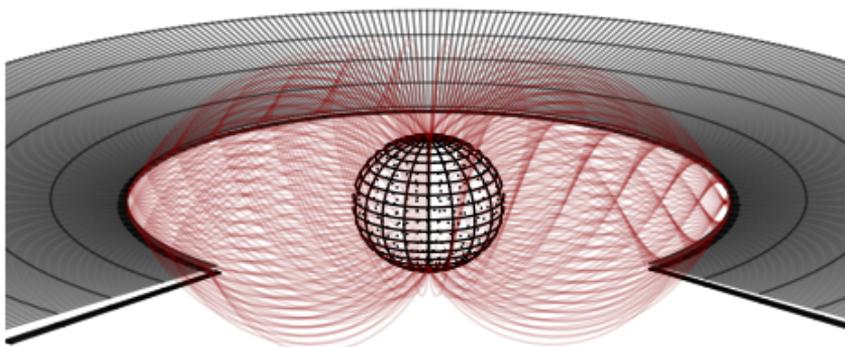
Figure 3.2: Schematic view of the two different accretion states. *Top:* Soft state with inner disk extending all the way down to the neutron star surface. *Bottom:* Hard state with truncated disk and hot inner flow (red).

radiation component. Depending on the mass accretion rate, the disk truncation radius varies and so the strength of the thermal disk and hot inner flow components can vary. To simplify, this means that hard state typically corresponds to a low accretion rate and soft state to a high mass accretion rate. In the quiescent state, the flow of matter might then come to a halt completely.

3.1.3 Boundary layers

Our simple analysis of accretion disk physics has shown that viscous dissipation can get rid of up to half of the potential energy of the incoming matter. Where the other half goes, we shall look next.

Imagine the accretion disk extending all the way down to the central star. The spin frequency of this disk edge can be taken to be Keplerian, $\Omega_K(R)/2\pi \sim$ 1500 Hz. The star, on the other hand, usually rotates anywhere from 100 to 600 revolutions per second.[127,128] Hence, we expect a thin interface between the star and the disk where angular velocity changes by a factor of $\sim$ 3 to 15. This region we call the boundary layer.

Let us assume a thin layer of width b so that $\Omega(R+b) \approx \Omega_K(R+b)$. Within this layer, the angular velocity should decrease to Ω_* as we move from radial location $R+b$ to R towards the star's surface. The viscous torque to spin up the star is then, similar to (3.21), written as

$$\tau_* = \dot{M}R^2(\Omega_K - \Omega_*). \tag{3.30}$$

Rate of the kinetic energy change, on the other hand, is simply obtained by considering the difference of the kinetic energies per time as

$$\dot{E} = \frac{1}{2}\dot{M}R^2(\Omega_K^2 - \Omega_*^2) = \frac{1}{2}\dot{M}\frac{GM}{R}\left[1 - \left(\frac{\Omega_*}{\Omega_K}\right)^2\right] \tag{3.31}$$

For the expression of the total rate of energy change we need to subtract the work done by the viscous torque per unit time, $\tau\Omega_*$, to get

$$L_{BL} = \frac{1}{2}\dot{M}R^2(\Omega_K^2 - \Omega_*^2) - \dot{M}R^2\Omega_*(\Omega_K - \Omega_*) = \frac{1}{2}\frac{GM\dot{M}}{R}\left(1 - \frac{\Omega_*}{\Omega_K}\right)^2 \tag{3.32}$$

In the limit $\Omega_* \ll \Omega_K$ we obtain

$$L_{BL} = \frac{1}{2}\frac{GM\dot{M}}{R} = \frac{1}{2}L_{acc}. \tag{3.33}$$

Let us finally estimate the temperature of this layer. By assuming an optically thick emitting region, we get a characteristic blackbody temperature again from

$$A_{BL}\sigma_{SB}T_{BL}^4 \sim L_{BL}, \tag{3.34}$$

where A_{BL} is the area of the emitting region. As a reasonable first guess we can use $b \sim H$ so an annulus around the star has an area of $A_{BL} = 2 \times 2\pi RH$ taking into account both top and bottom face. This corresponds to a temperature of

$$T_{BL} \sim \left(\frac{GM\dot{M}}{8\pi\sigma_{SB}R^2H}\right)^{1/4} \sim T_* \left(\frac{R}{H}\right)^{1/4} \tag{3.35}$$

As another option we can consider a so-called spreading layer.[129,130] Instead of assuming that the energy is dissipated in a thin equatorial ring, we can assume

that it will spread to cover the whole star. In this case, $A_{SL} \sim 4\pi R^2$, and using Eq. (3.34), we get

$$T_{SL} \sim T_*, \tag{3.36}$$

i.e., a smaller temperature ($T_{SL} < T_{BL}$) that is comparable to the temperature of the disk.

Finally, one should note that the physical processes discussed here assume Newtonian gravity. In a general relativistic treatment the energy release in the boundary layer can be almost two times that of the energy released in the disk.[131,132]
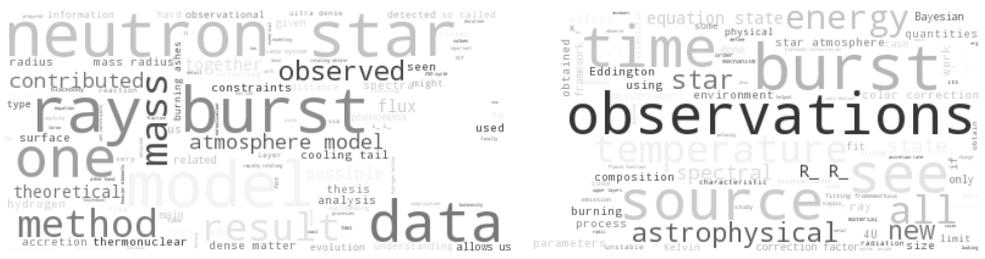
4 | **Probing the ultra-dense matter**

The main motivation for this thesis was to set constraints for equation of state of the ultra-dense matter inside neutron stars. Instead of starting from the nuclear physics that works on the smallest scales, we use astrophysical observations to study large-scale "global" aspects of neutron stars. It is then possible to make a step back to the nuclear physics because the size of a compact star is strongly coupled to the composition of its core.

Looking from the astrophysical point of view, it is the size of the neutron star that will define many of its observable features. One of the most important characteristics is the compactness of the object that will then define the exact shape of the spacetime surrounding it. The strongly curved spacetime, in turn, influences many of the phenomena occurring in the close vicinity of the star and will also leave its distinct imprints on the observations.

The physical phenomena behind the observable features, on the other hand, are often highly energetic, otherwise they would not be seen by distant observers, such as us. It is these highly energetic physical processes that will then render the neutron stars visible to us, and that at the same time carry a plethora of information from the surroundings of where they originated from. This gives birth to a beautiful connection where the delicate and unattainable nuclear physics of the ultra-dense matter is coupled to vigorous astrophysical phenomena that we can observe. The caveat here is that the astrophysical processes are often messy and poorly understood. Hence, a thorough understanding of both, the nature of the observed phenomena and how it exactly couples to the nuclear physics, is needed.

In this thesis, we will focus on extracting information from neutron stars using astrophysical phenomena called X-ray bursts. They are produced by an unstable thermonuclear runaways in the surface layers of the star and can be seen as end-results of accretion. In theory, using the X-ray bursts to probe the neutron star interiors is a robust way to study the matter inside the star as we can theoretically model the characteristics of the emerging radiation and these models can be applied to describe the data that we see. In practice, however, caution is needed when applying the models as the environment and the astrophysics near the neutron star play a huge role.

In this final chapter, we will lay out the basics of how observing the burst cooling it is possible to set constraints on the size of the emitting area, and in the end, on the radius of the neutron star. We will also summarize the content of the

articles in this thesis and discuss our work where we try to understand not only the complex role of the astrophysical surroundings but in the end, the composition of the core.

4.1   X-ray bursts and unstable thermonuclear burning

Accretion can be a powerful energy source but this is not the end of the material that slowly spirals down into the star. After it has traveled all the way to the surface of the neutron star, it will slowly sink and mix with the material in the star's upper layers. Here this new material compresses and heats up, acting as fresh fuel. Eventually the kinetic energy of the nuclei is large enough so that the protons will collide, fuse together, and release a fraction of their rest-mass energy. This heat injection will then start an unstoppable chain reaction that creates a burning front that eventually covers the whole star. Thermonuclear fusion reaction will then last until all the available fuel on the star's upper layers is exhausted and consumed. This is the basic picture of an unstable nuclear burning taking place in the neutron star's upper layers. One should also note that a stable, continuous burning is also possible via a similar mechanism. Generally, however, the nuclear burning reaction rates have a very strong temperature dependency, and hence, the plasma is very unstable for local perturbations that might then start the explosive burning.

The explosive burning front rapidly expands and momentarily engulfs the whole star. This hot shell will then cool down and shine X-rays to us. Observationally these bursts are classified as type-I X-ray bursts.[54,133] As another option, we might see flaring also from instabilities in the incoming mass flow. These events are classified as type-II bursts, and we do not focus on them, as here we are interested in probing the neutron star itself. A typical X-ray burst has a rise time of 0.1 to 10 seconds and a duration from 10 to 100 seconds. During this time, it releases $10^{39} - 10^{40}$ erg of energy. Temperature in the upper layers is of around $T \sim 10^7$ K and the main ingredient for the fusion process is either hydrogen, helium, or both.

The driving engine for an X-ray burst is the unstable thermonuclear fusion process.[134–136] The burning of hydrogen plasma is dominated by the CNO-cycle if temperature is around 10^7 K. For a slightly hotter plasma, $T \gtrsim 8 \times 10^7$ K, we have to modify the reaction a bit into a so-called hot CNO-cycle.[137] Helium plasma, on the other hand, burns via the triple-α process (active when $T \gtrsim 2 \times 10^8$ K). In addition to these two main reactions, the αp-process can operate when $T \gtrsim 5 \times 10^8$ K, creating heavier elements like Ne, Na, and Mg. The rp-process to synthesize even heavier elements can take place if $T \sim 10^9$ K. In the end, the accreted matter is fused together into heavier elements, and at the same time, energy is released into the neutron star envelope.

If the accreted material does not have any hydrogen, or if the hot CNO-cycle has enough time to burn all the available hydrogen into helium, the ignition starts in the helium shell. On the other hand, if the hot CNO burning of hydrogen is not continuous, it can trigger the runaway in the hydrogen shell, after which the helium shell will also ignite. These minor details have observational importance,

as we sometimes see bursts with very short rise times, and other times it might take seconds for the burst to really get going.

This discrepancy is believed to originate from this changing ignition mechanism. In addition to the normal type-I bursts, we have also recently detected more rare long-duration bursts, now commonly dubbed as "superbursts".[61,138,139] These are thought to be powered by carbon burning.[140] When looking at the duration, there are also a third class of bursts in between the superbursts and normal bursts, named "intermediate bursts".[141]

All in all, the energy production of bursts appears to be a complex mechanism that we do not fully understand yet.[142,143] This is also reflected in the large variety of burst durations, energetics, and rise times that we have observationally detected.[144]

4.2 Measuring the sizes of the bursting sources

Even though the bursts characteristics change from one burst to another as we saw in Sect. 4.1, the cooling appears to obey some common trends. This means that as long as we have some kind of energy injection deep below the neutron star's atmosphere, the energy will radiate out and the uppermost layers of the star will then shape it into a similar cooling curve, independent of the actual details of the injection. If we are then able to model the atmosphere and the processes therein, we can use the bursts as probes for the neutron star interiors. Note, however, that not every burst is powerful enough to be of practical use. As we shall see, we additionally require that the bursts reach the Eddington limit, which in practice means using the PRE-bursts only.

To begin, let us define three different families of quantities: observed quantities (obs), theoretical quantities predicted by our model at infinity (∞), and the same theoretical model quantities in the local frame of the star ($*$). This is done, because general relativistic effects change the local physical quantities as they travel from the star to a distant observer.[54] More specifically, we can connect the temperatures T, radii R, and luminosities L as

$$R_\infty = R_*(1 + z), \tag{4.1}$$

$$T_\infty = \frac{T_*}{1 + z}, \tag{4.2}$$

$$L_\infty = \frac{L_*}{(1 + z)^2}, \tag{4.3}$$

where $(1 + z)$ is the redshift factor that is related to the previously defined compactness $u = 2GM/Rc^2$ as

$$1 + z = (1 - u)^{-1/2}. \tag{4.4}$$

From the observations, we see that the detected burst spectra are reasonably well described by the Planck function (blackbody) as

$$F_{E,\text{obs}} \approx \pi B_E(T_\text{obs})K_\text{obs}, \tag{4.5}$$
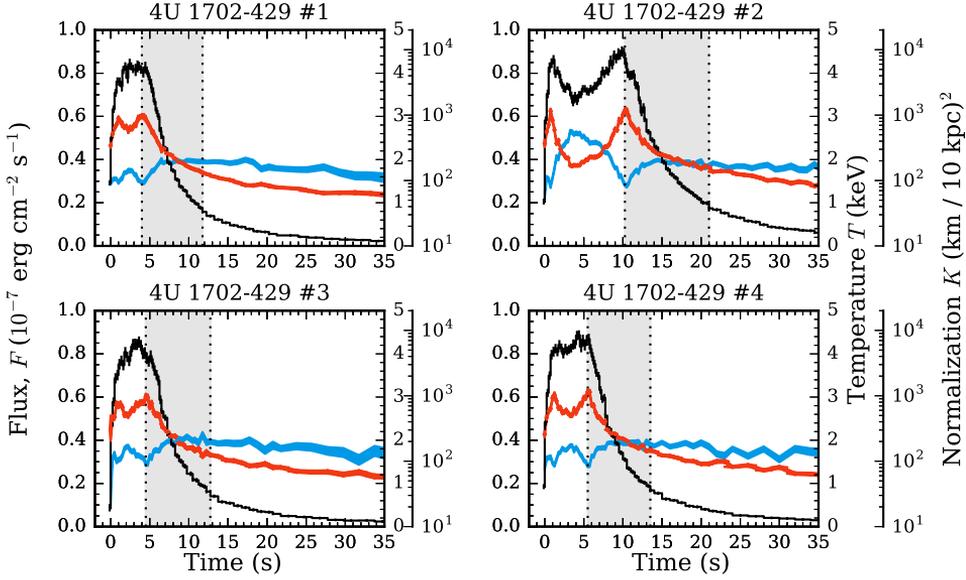
Figure 4.1: Examples of bolometric flux, temperature and blackbody normalization evolution during the hard-state PRE bursts. The black line shows the estimated bolometric flux (left-hand vertical axis) in units of 10^{-7} erg cm^{-2} s^{-1}. The blue ribbon shows the blackbody normalization (outer right-hand vertical axis) in $(\mathrm{km}/10\,\mathrm{kpc})^2$. The red ribbon shows the blackbody temperature (inner right-hand vertical axis) in keV. Highlighted gray area marks a typical region of the cooling tail used in the fitting procedures.

where $B_E(T_{\mathrm{obs}})$ is a blackbody function with a measured temperature T_{obs} and normalization K_{obs}, together with E which is the photon energy that we observe at. The normalization for an object at a distance D in the sky is

$$K_{\mathrm{obs}} = \frac{R^2_{\mathrm{obs}}}{D^2}. \tag{4.6}$$

Observed bolometric flux is then

$$F_{\mathrm{obs}} = \int_0^\infty F_{E,\mathrm{obs}}dE = \sigma_{\mathrm{SB}}T^4_{\mathrm{obs}}\frac{R^2_{\mathrm{obs}}}{D^2}. \tag{4.7}$$

Some examples of Planck function fit results for X-ray bursts are shown in Fig. 4.1. Here the time-dependent spectral fits are shown for one particular source, 4U 1702−429.[145,146] All of the bursts shown here are exhibiting the photospheric radius expansion, that can be seen from the characteristic dip in the normalization and of the simultaneous maximum in the temperature.[144] The flux corresponding to the exact moment when the photosphere collapses back to the neutron star's surface is dubbed the touchdown flux, and it is visualized by the first vertical dotted line in the figures.

From the atmosphere models of neutron stars, we obtain a similar result. The local detailed model spectra are well approximated by a so-called diluted black-body model given as

$$F_{E,*} \approx \pi w B_E(f_c T_{\text{eff},*}),$$ (4.8)

where w is the dilution factor, f_c is the color-correction factor, and $T_{\text{eff},*}$ is the effective temperature of the atmosphere. This allows us to connect the observed values to the theoretical model values by first redshifting these quantities to infinity. From (4.2) we simply obtain that the temperature of the model as seen by a distant observer must be

$$f_c T_{\text{eff},\infty} = f_c \frac{T_{\text{eff},*}}{1 + z}.$$ (4.9)

Similarly, the area of the star on the sky must be related not to R_* but to R_∞ as given by (4.1)

$$w\frac{R_\infty^2}{D^2} = w\frac{R_*^2(1 + z)^2}{D^2}.$$ (4.10)

The latter (4.10) gives immediate constraints for the radius as it can be equated with the observed size (4.6) as[147,148]

$$R_{\text{obs}}^2 = wR_\infty^2 = wR_*^2(1 + z)^2.$$ (4.11)

Additional constraints can be obtained by measuring the Eddington limit of the source. As we have seen, there exists a flux for which the radiation forces equal to the gravitational forces (see Sect. 2.2.3), given as

$$F_{\text{Edd},*} = \frac{GMc}{\kappa_T R_*^2}(1 + z),$$ (4.12)

where $\kappa_T = 0.2(1 + X)$ cm^2 g^{-1} is the Thomson electron scattering opacity and X is the hydrogen mass fraction. One should note here that even though we use the Thomson electron scattering opacity in the notation, one is not restricted to assuming this. It is, for example, possible to take the Klein-Nishina reduction in the cross-section into account which formally allows for super-Eddington fluxes.[71] In reality the Eddington limit is, of course, still respected. Using this characteristic flux we can also define the Eddington luminosity $L_{\text{Edd},*}$ and the corresponding Eddington temperature $T_{\text{Edd},*}$ as

$$L_{\text{Edd},*} = 4\pi R_*^2 F_{\text{Edd},*} = 4\pi R_*^2 \sigma_{\text{SB}} T_{\text{Edd},*}^4.$$ (4.13)

These are again quantities defined near the star whereas what one observes at infinity are given by

$$L_{\text{Edd},\infty} = \frac{L_{\text{Edd},*}}{(1 + z)^2},$$ (4.14)

$$F_{\text{Edd},\infty} = \frac{L_{\text{Edd},\infty}}{4\pi D^2} = \frac{GMc}{\kappa_T D^2}\frac{1}{1 + z},$$ (4.15)

and

$$T_{\mathrm{Edd},\infty} = \frac{T_{\mathrm{Edd},*}}{1 + z}. \tag{4.16}$$

As the simplest case, we can obtain additional constraints for the radius and mass by just measuring the $F_{\mathrm{Edd},\infty}$ somehow. This can be done, for example, by equating it with the touchdown flux obtained from the time-dependent burst spectra. This is the basis of the so-called "touchdown method".[148–151]

A more sophisticated version of this is the so-called "cooling tail method".[152,153] Here we can compute the varying color-correction factor f_{c} from the atmosphere models as a function of $\ell \equiv L_*/L_{\mathrm{Edd},*}$. In this case, the dilution factor was obtained from the approximative relation $f_{\mathrm{c}} \approx w^{-4}$. The color-correction factor can then be related to multiple K_{obs} measurements, each representing one time snapshot from the cooling tail. As the time passes and the surface cools down, the flux decreases. This allows us to compare the model dependency of ℓ vs. f_{c} to the observations of $F_{\mathrm{obs}}/F_{\mathrm{Edd},\infty}$ vs. $K_{\mathrm{obs}}^{-1/4}$. Hence, extra information from the observations is used because not only are the individual color-correction factor values compared against the model but also their full dynamic evolution as a function of flux is taken into account. The fitting procedure is two dimensional in this case as we fit $F_{\mathrm{Edd},\infty}$ and R_∞^2/D^2 as free parameters simultaneously. Interestingly, the combination of these two fit parameters then yield a distance-independent quantity, physically corresponding to the Eddington temperature of the source at infinity, given as

$$T_{\mathrm{Edd},\infty} = 1.14 \times 10^8 \left(\frac{F_{\mathrm{Edd},\infty}}{10^{-7}\ \mathrm{erg\,cm^{-2}\,s^{-1}}} \right)^{1/4} \left(\frac{(\mathrm{km}/10\,\mathrm{kpc})^2}{R_\infty^2/D^2} \right)^{1/4}\ \mathrm{K}. \tag{4.17}$$

This corresponds to a parametric relation for the M and R via the compactness u, given as

$$R = \frac{c^3 u(1-u)^{3/2}}{2\kappa_{\mathrm{T}}\sigma_{\mathrm{SB}}T_{\mathrm{Edd},\infty}^4} \approx 1188 \frac{u(1-u)^{3/2}}{(1+X)T_{\mathrm{Edd},\infty,7}^4}\ \mathrm{km},$$
$$M \approx u\frac{R}{2.95\,\mathrm{km}}\ \mathrm{M}_\odot, \tag{4.18}$$

where $T_{\mathrm{Edd},\infty,7} = T_{\mathrm{Edd},\infty}/10^7\,\mathrm{K}$. Later on, another variant of this method was introduced, called "direct cooling tail method" where the assumption of $f \approx w^{-4}$ was relaxed, i.e., both f_{c} and w are considered, and the fitting is done directly via the M, R and D parameters.[145,154]

The usage of these methods on X-ray burst data span almost three decades of scientific work as of now. Starting from the early work in the late 80s they have since improved and been applied to various sources to estimate the radius and mass. Latest in the family is the method of fitting the observed data directly with the atmosphere models.[146] Although computationally more demanding exercise, it allows us to finally extract every piece of information possible from the data. This is based on the additional model dependency on the surface gravity, composition, and detailed spectral shape that slightly deviates from the Planck function.

The big caveat here for any of the aforementioned methods is the surroundings. We have seen that the astrophysical environment of neutron stars can be very active and lively. In the general picture, we have the accretion as an energy source and the disk to dissipate this energy. The disk is, however, not a simple geometrically thin steady layer but can have complex inner flow. On the other hand, if the disk does extend all the way down to the star, an additional complication originates from the boundary or spreading layer that not only can cover the star but also radiate on its own. These are some of the complications that we face when trying to analyze our neutron star observations, as after all when trying to constrain the mass and radius of the star we must make sure that it is actually the star that we are looking at.

4.3 Scientific summary of the results

In this thesis, we have focused on constraining the equation of state of the cool ultra-dense matter inside neutron stars with astrophysical measurements. The main results are two-folded as we have both

- improved our understanding of ultra-dense matter and have been able to put stringent constraints on the equation of state of the neutron star interiors, and

- progressed our understanding of neutron star environments and astrophysics of X-ray burst.

To be able to do this, we had to develop our observational and statistical methods, do theoretical research in order to understand the astrophysical scenarios better, develop and improve our physical models, and finally apply these new methods and information to real-world observations. Because of this, the results and work in this thesis can be divided into three categories that we now discuss in more detail. In short, these include *1)* theoretical work on the models, *2)* understanding the astrophysical environment better, and *3)* applying the models and the new insights to astronomical observations.

4.3.1 Modeling of neutron star atmospheres and emergent radiation

Computing hot neutron star atmosphere models for the bursters is of paramount importance for obtaining the mass and radius measurements from the burst observations. More specifically, we are interested in the color correction factor f_c and the dilution factor w, in order to compare our knowledge to observations. Previous models for hot atmospheres have all assumed simple hydrogen, helium, or solar composition for the plasma. In some cases, however, the burning ashes may rise from the burning depths up to the photosphere, leading to the appearance of the metal absorption edges in the spectra. These effects may have a substantial impact on the color correction factor and the dilution factor w. In paper I, we have developed a new atmosphere modeling code to compute the emergent spectra for a composition consisting of any atomic species. We find that the metals may change f_c by up to about 40%. The presented models also made possible to determine the NS mass and radii more accurately for cases when we do see signs of burning

ashes, and provided a new tool to probe the nuclear burning mechanisms in X-ray bursts.

The radiative process that we consider all occur at or near the neutron star. Because of this, many general relativistic effects play an important role in shaping the observations. In paper II, a theoretical framework for emission originating from rapidly rotating oblate compact objects was described in detail. In order to solve the geodesic equation, a new split Hamilton-Jacobi formalism was constructed for a metric that is expanded up to second order in rotation and hence includes effects of light bending, frame-dragging, and quadrupole corrections for the photon trajectories. We also gave detailed descriptions of the numerical algorithms used and provide an open-source implementation of the numerical framework called BEN-DER. As an application, we study spectral line profiles from rapidly rotating oblate neutron stars. The Full Width at Tenth Maximum and Full Width at Half Maximum for the so-called smearing kernels are also reported for all of the possible viewing angles. These can be then used to quantitatively estimate the effects of rotational smearing on the observed spectra.

4.3.2 Understanding the astrophysical environments of X-ray bursts

As we have seen, the neutron star environment is an important factor that needs to be understood before reliable mass and radius estimates can be obtained from X-ray burst observations. In paper III, we study the effects of accretion for one particular source, LMXB system 4U 1608−52. We found a strong dependence of the burst properties on the flux and spectral hardness of the persistent emission before burst. Bursts occurring during the low accretion rate (hard) state exhibit evolution of the blackbody normalization consistent with the theoretical predictions of neutron star atmosphere models. However, bursts occurring during the high accretion rate (soft) state show roughly constant normalization, which is inconsistent with models and therefore these bursts cannot be easily used to determine neutron star parameters.

In the next paper IV, we continue our analysis further by studying 246 X-ray bursts in total, from 11 different LMXB systems. Again, we found a dependence between the persistent spectral properties and the time evolution of the blackbody normalization during the bursts. The neutron star atmosphere model predictions agree with the observations for most bursts occurring in hard, low-luminosity, spectral states, but rarely during soft, high-luminosity, states. We attributed the observed phenomena to the accretion flow, which can influence the cooling of the neutron star especially during the soft state when the accretion rate is high. The results had the important implication that only the bursts occurring in the hard, low-luminosity spectral states could be reliably used for mass and radius determination.

4.3.3 Constraining the mass and radius of neutron stars

By now applying the atmosphere model results to the X-ray burst data, we can try to set constraints for the size of the emitting source. However, here it is crucial

to take into account also the accretion rate, i.e., consider bursts that occur during the hard-state only. In paper V we did this analysis for three different LMXB systems: 4U 1702−429, 4U 1724−307, and SAX J1810.8−260. This allows us to set constraints for the masses, radii, compositions, and distances of the neutron stars in those systems. We then obtained a parameterized equation of state by comparing the resulting neutron star structures to the radius and mass measurements we had. This was done by solving the TOV-equations and then using Monte Carlo algorithm within a Bayesian framework to obtain constraints for the underlying equation of state parameters. This allows us to set limits on various nuclear parameters and to constrain an empirical pressure-density relationship for the dense matter. Our predicted equation of state leads to a neutron star radius between 10.5 to 12.8 km for a mass of $1.4\,M_\odot$.

The bursts that we considered in the aforementioned publication, were constrained to have an atmosphere consisting of almost fully of hydrogen and helium. This is always not the case as explosive nuclear burning can fuse H and He into heavier elements too. In paper VI, we presented our analysis of one particularly interesting long burst observed from the neutron star in LMXB system HETE J1900.1−2455. New atmosphere model fits to these bursts indicated that sometimes the photosphere can consist entirely of metals, i.e., nuclear burning ashes. These heavy metals like iron and nickel were detected already early on during the burst, which makes it possible that a radiatively driven wind might eject some of these ashes also into the interstellar space. Hence, neutron star X-ray bursts might be one possible source of interstellar pollution.

Most previous works on X-ray bursts have used the Planck functions as a proxy to simplify the model vs. data comparison. In paper VII, we, for the first time, fitted neutron star atmosphere models directly to the observed spectra. This was done using a new nested hierarchical Bayesian model that allowed us to set new limits on mass, radius, composition, and distance of the neutron star in 4U 1702−429. We then find a radius of $R = 12.4 \pm 0.4$ km, gravitational mass $M = 1.9 \pm 0.3\,M_\odot$, distance $5.1 < D/\mathrm{kpc} < 6.2$, and hydrogen mass fraction $X < 0.09$ with a 68% confidence for this source.

4.4 The author's contribution to the publications

Paper I.: Models of neutron star atmospheres enriched with nuclear burning ashes

The author contributed to the main idea of the paper, independently redesigned the neutron star atmosphere code used for the calculations, and implemented new physical processes to this numerical framework. The author also prepared most of the manuscript together with J. Kajava.

Paper II.: Radiation from rapidly rotating oblate neutron stars

The author proposed the idea of applying the split-Hamilton method to the ray tracing problem and designed the numerical code for the calculations. The theoretical framework and the related formulae were derived together with P. Pihajoki. The manuscript was also prepared together with P. Pihajoki.

Paper III.: The effect of accretion on the measurement of neutron star mass and radius in the low-mass X-ray binary 4U 1608–52

The author of the thesis made contributions to the manuscript, reduced and analyzed the observational X-ray data, and contributed to the scientific discussions related to the manuscript.

Paper IV.: The influence of accretion geometry on the spectral evolution during thermonuclear (type I) X-ray bursts

The author participated in the reduction and analysis of the observational data, made significant contributions to the development of the data reduction software, and helped in the preparation of the manuscript.

Paper V.: Equation of state constraints for the cold dense matter inside neutron stars using the cooling tail method

The author independently designed the Bayesian fitting framework for the cooling tail method, reduced and analyzed the X-ray observations, and finally led the equation of state modeling from the observations. The author also prepared the manuscript.

Paper VI.: Detection of burning ashes from thermonuclear X-ray bursts

The author contributed to the main idea of this research and was responsible of the atmosphere modeling of the observations. The Bayesian atmosphere spectral model fitting framework was also independently designed by the author. Author also contributed to the manuscript.

Paper VII.: Neutron star mass and radius measurements from atmospheric model fits to X-ray burst cooling tail spectra

The author independently designed the hierarchical Bayesian fitting framework, implemented it into a code together with M.C. Miller and A.W. Steiner, analyzed the data, and, finally, prepared most of the manuscript together with M.C. Miller.

5 | Bibliography

[1]   L. D. Landau. *Phys. Z. Sowjetunion*. 1, pp. 285–288. (1932). (See p. 1)
"On the theory of stars".

[2]   J. Chadwick. *Nature*. 129, p. 312. (1932). (See p. 2)
"Possible Existence of a Neutron"
DOI: `10.1038/129312a0`.

[3]   J. Chadwick. *Proceedings of the Royal Society of London Series A*. 136,
pp. 692–708. (1932). (See p. 2)
"The Existence of a Neutron"
DOI: `10.1098/rspa.1932.0112`.

[4]   E. Rutherford. *Proceedings of the Royal Society of London Series A*. 97,
pp. 374–400. (1920). (See p. 2)
"Bakerian Lecture. Nuclear Constitution of Atoms"
DOI: `10.1098/rspa.1920.0040`.

[5]   W. Baade & F. Zwicky. *Proceedings of the National Academy of Science*.
20, pp. 259–263. (1934). (See p. 2)
"Cosmic Rays from Super-novae"
DOI: `10.1073/pnas.20.5.259`.

[6]   W. Baade & F. Zwicky. *Physical Review*. 45, p. 138. (1934). (See p. 2)
"Supernovae and cosmic rays"
DOI: `10.1103/PhysRev.46.76.2`.

[7]   P. A. M. Dirac. *Proceedings of the Royal Society of London Series A*.
109, pp. 642–653. (1925). (See pp. 2, 24)
"The Fundamental Equations of Quantum Mechanics"
DOI: `10.1098/rspa.1925.0150`.

[8]   R. H. Fowler. *MNRAS*. 87, pp. 114–122. (1926). (See pp. 2, 24)
"On dense matter"
DOI: `10.1093/mnras/87.2.114`.

[9]   E. C. Stoner. *Philos. Mag.* 9, p. 944. (1930). (See pp. 3, 24, 28)
"The equilibrium of dense stars".

[10]   W. Anderson. *Zeitschrift für Physik*. 56. 11, pp. 851–856. (1929). (See pp. 3, 24)
"Über die Grenzdichte der Materie und der Energie"
DOI: `10.1007/BF01340146`.

[11]   S. Chandrasekhar. *MNRAS*. 91, pp. 456–466. (1931). (See pp. 3, 24)
"The highly collapsed configurations of a stellar mass"
DOI: `10.1093/mnras/91.5.456`.

[12]   D. G. Yakovlev. *Physics Uspekhi*. 37, pp. 609–612. (1994). (See p. 3)
"From the history of physics: The article by Ya I Frenkel' on 'binding forces' and the theory of white dwarfs"
DOI: `10.1070/PU1994v037n06ABEH000031`.

[13]   J. Frenkel. *Zeitschrift für Physik*. 47. 11, pp. 819–834. (1928). (See pp. 3, 24)
"Zur wellenmechanischen Theorie der metallischen Leitfähigkeit"
DOI: `10.1007/BF01328642`.

[14]   G. Gamow. *Physical Review*. 55, pp. 718–725. (1939). (See p. 3)
"Physical Possibilities of Stellar Evolution"
DOI: `10.1103/PhysRev.55.718`.

[15]   R. C. Tolman. *Physical Review*. 55, pp. 364–373. (1939). (See pp. 4, 33)
"Static Solutions of Einstein's Field Equations for Spheres of Fluid"
DOI: `10.1103/PhysRev.55.364`.

[16]   J. R. Oppenheimer & G. M. Volkoff. *Physical Review*. 55, pp. 374–381. (1939). (See pp. 4, 33)
"On Massive Neutron Cores"
DOI: `10.1103/PhysRev.55.374`.

[17]   G. Baym. "Neutron stars: the first fifty years". *The Neutron and its Applications, 1982*. Ed. by P. Schofield. 1982, pp. 45–50 (see p. 4).

[18]   A. S. Eddington. *The Internal Constitution of the Stars*. 1926 (see p. 4).

[19]   J. A. Wheeler. *ARA&A*. 4, p. 393. (1966). (See p. 5)
"Superdense Stars"
DOI: `10.1146/annurev.aa.04.090166.002141`.

[20]   A. G. Cameron. *ApJ*. 130, p. 884. (1959). (See p. 5)
"Neutron Star Models."
DOI: `10.1086/146780`.

[21]   R. C. Stabler. "Energy Loss Mechanisms from Very Dense Stars." PhD thesis. Cornell University., 1960 (see p. 5).

[22]   H.-Y. Chiu. *Annals of Physics*. 26, pp. 364–410. (1964). (See p. 5)
"Supernovae, neutrinos, and neutron stars"
DOI: `10.1016/0003-4916(64)90256-8`.

[23]   D. C. Morton. *Nature*. 201, pp. 1308–1309. (1964). (See p. 5)
"Neutron Stars as X-ray Sources"
DOI: `10.1038/2011308a0`.

[24]   H.-Y. Chiu & E. E. Salpeter. *Physical Review Letters*. 12, pp. 413–415.
(1964). (See p. 5)
"Surface X-Ray Emission from Neutron Stars"
DOI: `10.1103/PhysRevLett.12.413`.

[25]   J. N. Bahcall & R. A. Wolf. *Physical Review*. 140, pp. 1452–1466.
(1965). (See p. 5)
"Neutron Stars. II. Neutrino-Cooling and Observability"
DOI: `10.1103/PhysRev.140.B1452`.

[26]   J. N. Bahcall & R. A. Wolf. *ApJ*. 142, pp. 1254–1256. (1965). (See p. 5)
"An Observational Test of Theories of Neutron-Star Cooling."
DOI: `10.1086/148395`.

[27]   S. Tsuruta & A. G. W. Cameron. *Canadian Journal of Physics*. 44,
p. 1863. (1966). (See p. 5)
"Cooling and detectability of neutron stars"
DOI: `10.1139/p66-156`.

[28]   R. Giacconi, H. Gursky, F. R. Paolini & B. B. Rossi. *Physical Review
Letters*. 9, pp. 439–443. (1962). (See p. 5)
"Evidence for x Rays From Sources Outside the Solar System"
DOI: `10.1103/PhysRevLett.9.439`.

[29]   I. S. Shklovsky. *ApJ*. 148, p. L1. (1967). (See p. 6)
"On the Nature of the Source of X-Ray Emission of SCO XR-1."
DOI: `10.1086/180001`.

[30]   J. H. Oort. "The letters and papers of Jan Hendrik Oort as archived in
the University Library. Leiden". Ed. by J. K. Katgert-Merkelijn. Vol. 213.
Astrophysics and Space Science Library. 1997. DOI: `10.1007/978-94-011-5764-3` (see p. 6).

[31]   K. Lundmark. *PASP*. 33, p. 225. (1921). (See p. 6)
"Suspected New Stars Recorded in Old Chronicles and Among Recent
Meridian Observations"
DOI: `10.1086/123101`.

[32]   N. U. Mayall. *Leaflet of the Astronomical Society of the Pacific*. 3, p. 145.
(1939). (See p. 6)
"The Crab Nebula, a Probable Supernova".

[33] D. A. Green & F. R. Stephenson. "Historical Supernovae". *Supernovae and Gamma-Ray Bursters*. Ed. by K. Weiler. Vol. 598. Lecture Notes in Physics, Berlin Springer Verlag. 2003, pp. 7–19. DOI: `10.1007/3-540-45863-8_2` (see p. 6).

[34] W. Baade. *ApJ*. 96, p. 188. (1942). (See p. 6)
"The Crab Nebula."
DOI: `10.1086/144446`.

[35] R. Minkowski. *ApJ*. 96, p. 199. (1942). (See p. 6)
"The Crab Nebula."
DOI: `10.1086/144447`.

[36] J. G. Bolton, G. J. Stanley & O. B. Slee. *Nature*. 164, pp. 101–102. (1949). (See p. 6)
"Positions of Three Discrete Sources of Galactic Radio-Frequency Radiation"
DOI: `10.1038/164101b0`.

[37] V. A. Dombrovsky. *Doklady Akad. Nauk SSSR*. 94, p. 1021. (1954). (See p. 6)

DOI: `10.1086/148028`.

[38] L. Woltjer. *ApJ*. 140, pp. 1309–1313. (1964). (See p. 6)
"X-Rays and Type I Supernova Remnants."
DOI: `10.1086/148028`.

[39] V. L. Ginzburg. *Soviet Physics Doklady*. 9, p. 329. (1964). (See p. 6)
"The Magnetic Fields of Collapsing Masses and the Nature of Superstars".

[40] S. Bowyer, E. T. Byram, T. A. Chubb & H. Friedman. *Nature*. 201, pp. 1307–1308. (1964). (See p. 6)
"X-ray Sources in the Galaxy"
DOI: `10.1038/2011307a0`.

[41] S. Bowyer, E. T. Byram, T. A. Chubb & H. Friedman. *Science*. 146, pp. 912–917. (1964). (See p. 6)
"Lunar Occultation of X-ray Emission from the Crab Nebula"
DOI: `10.1126/science.146.3646.912`.

[42] N. S. Kardashev. *AZh*. 41, p. 807. (1964). (See p. 6)
"Magnetic Collapse and the Nature of Intense Sources of Cosmic Radio-Frequency Emission".

[43] F. Pacini. *Nature*. 216, pp. 567–568. (1967). (See pp. 6, 7)
"Energy Emission from a Neutron Star"
DOI: `10.1038/216567a0`.

[44]   A. Hewish, S. J. Bell, J. D. H. Pilkington, P. F. Scott & R. A. Collins. *Nature*. 217, pp. 709–713. (1968). (See p. 7)
"Observation of a Rapidly Pulsating Radio Source"
DOI: 10.1038/217709a0.

[45]   T. Gold. *Nature*. 218, pp. 731–732. (1968). (See p. 7)
"Rotating Neutron Stars as the Origin of the Pulsating Radio Sources"
DOI: 10.1038/218731a0.

[46]   J. M. Comella, H. D. Craft, R. V. E. Lovelace & J. M. Sutton. *Nature*. 221, pp. 453–454. (1969). (See p. 7)
"Crab Nebula Pulsar NP 0532"
DOI: 10.1038/221453a0.

[47]   J. Grindlay, H. Gursky, H. Schnopper, D. R. Parsignault, J. Heise, A. C. Brinkman & J. Schrijver. *ApJ*. 205, pp. L127–L130. (1976). (See p. 7)
"Discovery of intense X-ray bursts from the globular cluster NGC 6624"
DOI: 10.1086/182105.

[48]   R. D. Belian, J. P. Conner & W. D. Evans. *ApJ*. 206, pp. L135–L138. (1976). (See p. 8)
"The discovery of X-ray bursts from a region in the constellation Norma"
DOI: 10.1086/182151.

[49]   G. W. Clark, J. G. Jernigan, H. Bradt, C. Canizares, W. H. G. Lewin, F. K. Li, W. Mayer, J. McClintock & H. Schnopper. *ApJ*. 207, pp. L105–L108. (1976). (See p. 8)
"Recurrent brief X-ray bursts from the globular cluster NGC 6624"
DOI: 10.1086/182190.

[50]   R. D. Belian, J. P. Conner & W. D. Evans. *ApJ*. 171, p. L87. (1972). (See p. 8)
"A Probable Precursor to the X-Ray Nova Centaurus XR-4"
DOI: 10.1086/180874.

[51]   O. P. Babushkina, M. I. Kudriavtsev, A. S. Melioranskii, I. A. Savenko, B. I. Iushkov & L. S. Bratoliubova-Tsulukidze. *Soviet Astronomy Letters*. 1, pp. 32–34. (1975). (See p. 8)
"Hard X-ray bursts in June 1971".

[52]   C. J. Hansen & H. M. van Horn. *ApJ*. 195, pp. 735–741. (1975). (See p. 8)
"Steady-state nuclear fusion in accreting neutron-star envelopes"
DOI: 10.1086/153375.

[53]   L. Maraschi & A. Cavaliere. "X-ray bursts of nuclear origin?" *X-ray Binaries and Compact Objects*. Ed. by K. A. van der Hucht. 1977, pp. 127–128 (see p. 8).

[54]   W. H. G. Lewin, J. van Paradijs & R. E. Taam. *SSRv*. 62, pp. 223–389. (1993). (See pp. 8, 48, 49)
"X-Ray Bursts"
DOI: 10.1007/BF00196124.

[55]   S. E. Woosley & R. E. Taam. *Nature*. 263, pp. 101–103. (1976). (See p. 8)
"Gamma-ray bursts from thermonuclear explosions on neutron stars"
DOI: 10.1038/263101a0.

[56]   J. van Paradijs, F. Verbunt, T. van der Linden, H. Pedersen & W. Wamsteker. *ApJ*. 241, pp. L161–L164. (1980). (See p. 8)
"Spectroscopic observations of the optical counterpart of Centaurus X-4"
DOI: 10.1086/183382.

[57]   J. Thorstensen, P. Charles & S. Bowyer. *ApJ*. 220, pp. L131–L134. (1978). (See p. 8)
"The optical counterpart of Aquila X-1 3U 1908+00"
DOI: 10.1086/182651.

[58]   E. P. Mazets, S. V. Golenotskii, V. N. Ilinskii, R. L. Aptekar & I. A. Guryan. *Nature*. 282, pp. 587–589. (1979). (See p. 8)
"Observations of a flaring X-ray pulsar in Dorado"
DOI: 10.1038/282587a0.

[59]   R. C. Duncan & C. Thompson. *ApJ*. 392, pp. L9–L13. (1992). (See p. 8)
"Formation of very strongly magnetized neutron stars - Implications for gamma-ray bursts"
DOI: 10.1086/186413.

[60]   D. C. Backer, S. R. Kulkarni, C. Heiles, M. M. Davis & W. M. Goss. *Nature*. 300, pp. 615–618. (1982). (See p. 8)
"A millisecond pulsar"
DOI: 10.1038/300615a0.

[61]   R. Cornelisse, J. Heise, E. Kuulkers, F. Verbunt & J. J. M. in't Zand. *A&A*. 357, pp. L21–L24. (2000). (See pp. 8, 49)
"The longest thermonuclear X-ray burst ever observed?. A BeppoSAX Wide Field Camera observation of 4U 1735-44".

[62]   V. E. Zavlin & G. G. Pavlov. "Modeling Neutron Star Atmospheres". *Neutron Stars, Pulsars, and Supernova Remnants*. Ed. by W. Becker, H. Lesch & J. Trümper. 2002, p. 263. eprint: astro-ph/0206025 (see pp. 15, 16).

[63]   A. Y. Potekhin. *Physics Uspekhi*. 57, pp. 735–770. (2014). (See pp. 15, 16)
"Atmospheres and radiating surfaces of neutron stars"
DOI: 10.3367/UFNe.0184.201408a.0793.

[64]   C. Alcock & A. Illarionov. *ApJ*. 235, pp. 534–553. (1980). (See p. 15)
"The surface chemistry of stars. I - Diffusion of heavy ions in white dwarf
envelopes. II - Fractionated accretion of interstellar matter"
DOI: `10.1086/157656`.

[65]   C. W. Misner, K. S. Thorne & J. A. Wheeler. *Gravitation*. 1973 (see p. 16).

[66]   R. M. Wald. *General relativity*. 1984 (see p. 16).

[67]   K. R. Pechenick, C. Ftaclas & J. M. Cohen. *ApJ*. 274, pp. 846–857.
(1983). (See p. 16)
"Hot spots on neutron stars - The near-field gravitational lens"
DOI: `10.1086/161498`.

[68]   R. A. London, W. M. Howard & R. E. Taam. *ApJ*. 287, pp. L27–L30.
(1984). (See p. 17)
"The spectra of X-ray bursting neutron stars"
DOI: `10.1086/184390`.

[69]   R. A. London, R. E. Taam & W. M. Howard. *ApJ*. 306, pp. 170–182.
(1986). (See p. 17)
"Model atmospheres for X-ray bursting neutron stars"
DOI: `10.1086/164330`.

[70]   I. I. Lapidus & R. A. Sunyaev. *MNRAS*. 217, pp. 291–303. (1985). (See
p. 17)
"Angular distribution and polarization of X-ray-burster radiation (during
stationary and flash phases)"
DOI: `10.1093/mnras/217.2.291`.

[71]   V. Suleimanov, J. Poutanen & K. Werner. *A&A*. 545, A120. (2012). (See
pp. 17, 51)
"X-ray bursting neutron star atmosphere models using an exact relativistic
kinetic equation for Compton scattering"
DOI: `10.1051/0004-6361/201219480`.

[72]   J. Nättilä, V. F. Suleimanov, J. J. E. Kajava & J. Poutanen. *A&A*. 581,
A83. (2015). (See p. 17)
"Models of neutron star atmospheres enriched with nuclear burning ashes"
DOI: `10.1051/0004-6361/201526512`.

[73]   G. B. Rybicki & A. P. Lightman. *Radiative processes in astrophysics*. New
York: Wiley-Interscience, 1979 (see p. 19).

[74]   J. Frank, A. King & D. J. Raine. *Accretion Power in Astrophysics*. Cam-
bridge: Cambridge University Press, Feb. 2002 (see pp. 19, 37, 40).

[75]   D. Mihalas & B. W. Mihalas. *Foundations of radiation hydrodynamics*.
1984 (see p. 20).

[76]   J. Poutanen. *ApJ*. 835, p. 119. (2017). (See p. 20)
"Rosseland and Flux Mean Opacities for Compton Scattering"
DOI: `10.3847/1538-4357/835/2/119`.

[77]   P. Haensel, A. Y. Potekhin & D. G. Yakovlev. *Neutron Stars 1 : Equation of State and Structure*. Vol. 326. Astrophysics and Space Science Library. New York: Springer, 2007 (see pp. 20, 24).

[78]   N. Chamel & P. Haensel. *Living Reviews in Relativity*. 11, p. 10. (2008). (See p. 20)
"Physics of Neutron Star Crusts"
DOI: `10.12942/lrr-2008-10`.

[79]   C. Bertulani & J. Piekarewicz. *Neutron Star Crust*. Space Science, Exploration and Policies Series. Nova Science Publishers, 2012. ISBN: 9781620819029 (see p. 20).

[80]   M. E. Caplan & C. J. Horowitz. *ArXiv e-prints*. (2016). (See p. 21)
"Astromaterial Science and Nuclear Pasta".

[81]   L. D. Landau & E. M. Lifshitz. *Statistical physics. Pt.1, Pt.2*. 1980 (see pp. 21, 24, 26, 27).

[82]   A. C. Phillips. *The physics of stars*. 1994 (see p. 23).

[83]   S. Chandrasekhar. *An introduction to the study of stellar structure*. 1939 (see pp. 24, 28).

[84]   E. L. Schatzman. *White dwarfs*. 1958 (see p. 24).

[85]   E. E. Salpeter. *ApJ*. 134, p. 669. (1961). (See p. 24)
"Energy and Pressure of a Zero-Temperature Plasma."
DOI: `10.1086/147194`.

[86]   R. F. Tooper. *ApJ*. 156, p. 1075. (1969). (See p. 24)
"On the Equation of State of a Relativistic Fermi-Dirac Gas at High Temperatures"
DOI: `10.1086/150036`.

[87]   Y. B. Zeldovich & I. D. Novikov. *Relativistic astrophysics. Vol.1: Stars and relativity*. 1971 (see p. 24).

[88]   S. I. Blinnikov. *Soviet Astronomy Letters*. 13, p. 346. (1987). (See p. 24)
"Thermodynamics of a Relativistic Fermi Gas".

[89]   D. G. Yakovlev & D. A. Shalybkov. *Astrophysics and Space Physics Reviews*. 7, p. 311. (1989). (See pp. 24, 26, 28)
"Degenerate Cores of White Dwarfs and Envelopes of Neutron Stars - Thermodynamics and Plasma Screening in Thermonuclear Reactions".

[90]   P. Debye & E. Hückel. *Physikalische Zeitschrift*. 24, pp. 185–206. (1923). (See p. 27)
"The theory of electrolytes. I. Lowering of freezing point and related phenomena".

[91]   S. L. Shapiro & S. A. Teukolsky. *Black holes, white dwarfs, and neutron stars: The physics of compact objects*. 1983 (see p. 27).

[92]   D. R. Dewitt, R. Schuch, H. Gao, W. Zong, S. Asp, C. Biedermann, M. H. Chen & N. R. Badnell. *Phys. Rev. A*. 53, pp. 2327–2336. (1996). (See p. 27)
"Dielectronic recombination of boronlike argon"
DOI: 10.1103/PhysRevA.53.2327.

[93]   S. Chandrasekhar. *MNRAS*. 95, pp. 226–260. (1935). (See p. 28)
"Stellar configurations with degenerate cores"
DOI: 10.1093/mnras/95.3.226.

[94]   F. Hund. *Zeitschrift fur Physik*. 99, pp. 119–136. (1936). (See p. 29)
"Über den Zusammenhang zwischen der Symmetrie eines Kristallgitters und den Zuständen seiner Elektronen"
DOI: 10.1007/BF01847819.

[95]   J. S. Read, C. Markakis, M. Shibata, K. Uryū, J. D. E. Creighton & J. L. Friedman. *Phys. Rev. D*. 79. 12, p. 124033. (2009). (See pp. 30, 31)
"Measuring the neutron star equation of state with gravitational wave observations"
DOI: 10.1103/PhysRevD.79.124033.

[96]   J. M. Lattimer & M. Prakash. *ApJ*. 550, pp. 426–442. (2001). (See p. 31)
"Neutron Star Structure and the Equation of State"
DOI: 10.1086/319702.

[97]   M. Bejger, T. Bulik & P. Haensel. *MNRAS*. 364, pp. 635–639. (2005). (See p. 31)
"Constraints on the dense matter equation of state from the measurements of PSR J0737-3039A moment of inertia and PSR J0751+1807 mass"
DOI: 10.1111/j.1365-2966.2005.09575.x.

[98]   B. D. Lackey, M. Nayyar & B. J. Owen. *Phys. Rev. D*. 73. 2, p. 024021. (2006). (See p. 31)
"Observational constraints on hyperons in neutron stars"
DOI: 10.1103/PhysRevD.73.024021.

[99]   P. B. Demorest, T. Pennucci, S. M. Ransom, M. S. E. Roberts & J. W. T. Hessels. *Nature*. 467, pp. 1081–1083. (2010). (See p. 31)
"A two-solar-mass neutron star measured using Shapiro delay"
DOI: 10.1038/nature09466.

[100]   J. Antoniadis, P. C. C. Freire, N. Wex, T. M. Tauris, R. S. Lynch, M. H. van Kerkwijk, M. Kramer, C. Bassa, V. S. Dhillon, T. Driebe, J. W. T. Hessels, V. M. Kaspi, V. I. Kondratiev, N. Langer, T. R. Marsh, M. A. McLaughlin, T. T. Pennucci, S. M. Ransom, I. H. Stairs, J. van Leeuwen, J. P. W. Verbiest & D. G. Whelan. *Science*. 340, p. 448. (2013). (See p. 31) "A Massive Pulsar in a Compact Relativistic Binary" DOI: 10.1126/science.1233232.

[101]   E. Fonseca, T. T. Pennucci, J. A. Ellis, I. H. Stairs, D. J. Nice, S. M. Ransom, P. B. Demorest, Z. Arzoumanian, K. Crowter, T. Dolch, R. D. Ferdman, M. E. Gonzalez, G. Jones, M. L. Jones, M. T. Lam, L. Levin, M. A. McLaughlin, K. Stovall, J. K. Swiggum & W. Zhu. *ApJ*. 832, p. 167. (2016). (See p. 31) "The NANOGrav Nine-year Data Set: Mass and Geometric Measurements of Binary Millisecond Pulsars" DOI: 10.3847/0004-637X/832/2/167.

[102]   F. Douchin & P. Haensel. *A&A*. 380, pp. 151–167. (2001). (See p. 31) "A unified equation of state of dense matter and neutron star structure" DOI: 10.1051/0004-6361:20011402.

[103]   A. Akmal, V. R. Pandharipande & D. G. Ravenhall. *Phys. Rev. C*. 58, pp. 1804–1828. (1998). (See p. 31) "Equation of state of nucleon matter and neutron star structure" DOI: 10.1103/PhysRevC.58.1804.

[104]   R. B. Wiringa, V. Fiks & A. Fabrocini. *Phys. Rev. C*. 38, pp. 1010–1037. (1988). (See p. 31) "Equation of state for dense nucleon matter" DOI: 10.1103/PhysRevC.38.1010.

[105]   L. Engvik, E. Osnes, M. Hjorth-Jensen, G. Bao & E. Ostgaard. *ApJ*. 469, p. 794. (1996). (See p. 31) "Asymmetric Nuclear Matter and Neutron Star Properties" DOI: 10.1086/177827.

[106]   H. Müther, M. Prakash & T. L. Ainsworth. *Physics Letters B*. 199, pp. 469–474. (1987). (See p. 31) "The nuclear symmetry energy in relativistic Brueckner-Hartree-Fock calculations" DOI: 10.1016/0370-2693(87)91611-X.

[107]   H. Müller & B. D. Serot. *Nuclear Physics A*. 606, pp. 508–537. (1996). (See p. 31) "Relativistic mean-field theory and the high-density nuclear equation of state" DOI: 10.1016/0375-9474(96)00187-X.

[108]   M. Alford, M. Braby, M. Paris & S. Reddy. *ApJ*. 629, pp. 969–978. (2005). (See p. 31)
"Hybrid Stars that Masquerade as Neutron Stars"
DOI: `10.1086/430902`.

[109]   T. M. Tauris & E. P. J. van den Heuvel. "Formation and evolution of compact stellar X-ray sources". *Compact stellar X-ray sources*. Ed. by W. H. G. Lewin & M. van der Klis. Apr. 2006, pp. 623–665 (see p. 38).

[110]   A. R. Choudhuri. *The physics of fluids and plasmas : an introduction for astrophysicists*. Nov. 1998 (see pp. 38, 40).

[111]   P. Podsiadlowski, S. Rappaport & E. D. Pfahl. *ApJ*. 565, pp. 1107–1133. (2002). (See p. 38)
"Evolutionary Sequences for Low- and Intermediate-Mass X-Ray Binaries"
DOI: `10.1086/324686`.

[112]   D. A. Leahy & J. C. Leahy. *Computational Astrophysics and Cosmology*. 2, p. 4. (2015). (See p. 38)
"A calculator for Roche lobe properties"
DOI: `10.1186/s40668-015-0008-8`.

[113]   S. Chapman & T.G. Cowling. *The Mathematical Theory of Non-uniform Gases: An Account of the Kinetic Theory of Viscosity, Thermal Conduction and Diffusion in Gases*. Cambridge Mathematical Library. Cambridge University Press, 1970. ISBN: 9780521408448 (see p. 41).

[114]   E. P. Velikhov. *Soviet Physics JETP*. 36, pp. 1398–1404. (1959). (See p. 41)
"Stability of an Ideally Conducting Liquid Flowing Between Cylinders Rotating in a Magnetic Field".

[115]   S. Chandrasekhar. *Proceedings of the National Academy of Science*. 46, pp. 253–257. (1960). (See p. 41)
"The Stability of Non-Dissipative Couette Flow in Hydromagnetics"
DOI: `10.1073/pnas.46.2.253`.

[116]   S. A. Balbus & J. F. Hawley. *ApJ*. 376, pp. 214–233. (1991). (See p. 41)
"A powerful local shear instability in weakly magnetized disks. I - Linear analysis. II - Nonlinear evolution"
DOI: `10.1086/170270`.

[117]   N. I. Shakura & R. A. Sunyaev. *A&A*. 24, pp. 337–355. (1973). (See p. 41)
"Black holes in binary systems. Observational appearance."

[118]   C. Done, M. Gierliński & A. Kubota. *A&A Rev.* 15, pp. 1–66. (2007). (See p. 43)
"Modelling the behaviour of accretion flows in X-ray binaries. Everything you always wanted to know about accretion but were afraid to ask"
DOI: `10.1007/s00159-007-0006-1`.

[119]   K. Mitsuda, H. Inoue, N. Nakamura & Y. Tanaka. *PASJ*. 41, pp. 97–111. (1989). (See p. 43)
"Luminosity-related changes of the energy spectrum of X1608-522".

[120]   G. Hasinger & M. van der Klis. *A&A*. 225, pp. 79–96. (1989). (See p. 43)
"Two patterns of correlated X-ray timing and spectral behaviour in low-mass X-ray binaries".

[121]   M. Gierliński & C. Done. *MNRAS*. 337, pp. 1373–1380. (2002). (See p. 43)
"The X-ray spectrum of the atoll source 4U 1608-52"
DOI: `10.1046/j.1365-8711.2002.06009.x`.

[122]   T. J. Maccarone & P. S. Coppi. *MNRAS*. 338, pp. 189–196. (2003). (See p. 43)
"Hysteresis in the light curves of soft X-ray transients"
DOI: `10.1046/j.1365-8711.2003.06040.x`.

[123]   T. Muñoz-Darias, R. P. Fender, S. E. Motta & T. M. Belloni. *MNRAS*. 443, pp. 3270–3283. (2014). (See p. 43)
"Black hole-like hysteresis and accretion states in neutron star low-mass X-ray binaries"
DOI: `10.1093/mnras/stu1334`.

[124]   M. Gierliński, A. A. Zdziarski, J. Poutanen, P. S. Coppi, K. Ebisawa & W. N. Johnson. *MNRAS*. 309, pp. 496–512. (1999). (See p. 43)
"Radiation mechanisms and geometry of Cygnus X-1 in the soft state"
DOI: `10.1046/j.1365-8711.1999.02875.x`.

[125]   M. L. McConnell, J. M. Ryan, W. Collmar, V. Schönfelder, H. Steinle, A. W. Strong, H. Bloemen, W. Hermsen, L. Kuiper, K. Bennett, B. F. Phlips & J. C. Ling. *ApJ*. 543, pp. 928–937. (2000). (See p. 43)
"A High-Sensitivity Measurement of the MeV Gamma-Ray Spectrum of Cygnus X-1"
DOI: `10.1086/317128`.

[126]   A. A. Zdziarski & M. Gierliński. *Progress of Theoretical Physics Supplement*. 155, pp. 99–119. (2004). (See p. 43)
"Radiative Processes, Spectral States and Variability of Black-Hole Binaries"
DOI: `10.1143/PTPS.155.99`.

[127]   A. L. Watts. *ARA&A*. 50, pp. 609–640. (2012). (See p. 45)
"Thermonuclear Burst Oscillations"
DOI: `10.1146/annurev-astro-040312-132617`.

[128]   A. Papitto, D. F. Torres, N. Rea & T. M. Tauris. *A&A*. 566, A64. (2014).
(See p. 45)
"Spin frequency distributions of binary millisecond pulsars"
DOI: `10.1051/0004-6361/201321724`.

[129]   N. A. Inogamov & R. A. Sunyaev. *Astronomy Letters*. 25, pp. 269–293.
(1999). (See p. 45)
"Spread of matter over a neutron-star surface during disk accretion".

[130]   V. Suleimanov & J. Poutanen. *MNRAS*. 369, pp. 2036–2048. (2006).
(See p. 45)
"Spectra of the spreading layers on the neutron star surface and constraints
on the neutron star equation of state"
DOI: `10.1111/j.1365-2966.2006.10454.x`.

[131]   R. A. Syunyaev & N. I. Shakura. *Soviet Astronomy Letters*. 12, pp. 117–
120. (1986). (See p. 46)
"Disk Accretion onto a Weak Field Neutron Star - Boundary Layer Disk
Luminosity Ratio".

[132]   N. R. Sibgatullin & R. A. Sunyaev. *Astronomy Letters*. 26, pp. 699–724.
(2000). (See p. 46)
"Energy Release During Disk Accretion onto a Rapidly Rotating Neutron
Star"
DOI: `10.1134/1.1323277`.

[133]   T. Strohmayer & L. Bildsten. "New views of thermonuclear bursts". *Com-
pact Stellar X-ray Sources*. Ed. by W. Lewin & M. van der Klis. Nov. 2010,
p. 113 (see p. 48).

[134]   M. Y. Fujimoto, T. Hanawa & S. Miyaji. *ApJ*. 247, pp. 267–278. (1981).
(See p. 48)
"Shell flashes on accreting neutron stars and X-ray bursts"
DOI: `10.1086/159034`.

[135]   R. K. Wallace & S. E. Woosley. *ApJS*. 45, pp. 389–420. (1981). (See
p. 48)
"Explosive hydrogen burning"
DOI: `10.1086/190717`.

[136]   J. L. Fisker, H. Schatz & F.-K. Thielemann. *ApJS*. 174, pp. 261–276.
(2008). (See p. 48)
"Explosive Hydrogen Burning during Type I X-Ray Bursts"
DOI: `10.1086/521104`.

[137] W. A. Fowler & F. Hoyle. *Nucleosynthesis in massive stars and super-novae*. 1965 (see p. 48).

[138] E. Kuulkers, J. J. M. in't Zand, M. H. van Kerkwijk, R. Cornelisse, D. A. Smith, J. Heise, A. Bazzano, M. Cocchi, L. Natalucci & P. Ubertini. *A&A*. 382, pp. 503–512. (2002). (See p. 49)
"A half-a-day long thermonuclear X-ray burst from KS 1731-260"
DOI: `10.1051/0004-6361:20011654`.

[139] T. E. Strohmayer & E. F. Brown. *ApJ*. 566, pp. 1045–1059. (2002). (See p. 49)
"A Remarkable 3 Hour Thermonuclear Burst from 4U 1820-30"
DOI: `10.1086/338337`.

[140] A. Cumming & L. Bildsten. *ApJ*. 559, pp. L127–L130. (2001). (See p. 49)
"Carbon Flashes in the Heavy-Element Ocean on Accreting Neutron Stars"
DOI: `10.1086/323937`.

[141] A. Cumming, J. Macbeth, J. J. M. in 't Zand & D. Page. *ApJ*. 646, pp. 429–451. (2006). (See p. 49)
"Long Type I X-Ray Bursts and Neutron Star Interior Physics"
DOI: `10.1086/504698`.

[142] J. Kuuttila, J. J. E. Kajava, J. Nättilä, S. E. Motta, C. Sánchez-Fernández, E. Kuulkers, A. Cumming & J. Poutanen. *A&A*. 604, A77. (2017). (See p. 49)
"Flux decay during thermonuclear X-ray bursts analysed with the dynamic power-law index method"
DOI: `10.1051/0004-6361/201730823`.

[143] J. J. M. in't Zand, M. E. B. Visser, D. K. Galloway, J. Chenevez, L. Keek, E. Kuulkers, C. Sánchez-Fernández & H. Wörpel. *A&A*. 606, A130. (2017). (See p. 49)
"Neutron star cooling and the rp process in thermonuclear X-ray bursts"
DOI: `10.1051/0004-6361/201731281`.

[144] D. K. Galloway, M. P. Muno, J. M. Hartman, D. Psaltis & D. Chakrabarty. *ApJS*. 179, pp. 360–422. (2008). (See pp. 49, 50)
"Thermonuclear (Type I) X-Ray Bursts Observed by the Rossi X-Ray Timing Explorer"
DOI: `10.1086/592044`.

[145] J. Nättilä, A. W. Steiner, J. J. E. Kajava, V. F. Suleimanov & J. Poutanen. *A&A*. 591, A25. (2016). (See pp. 50, 52)
"Equation of state constraints for the cold dense matter inside neutron

stars using the cooling tail method"
DOI: 10.1051/0004-6361/201527416.

[146]   J. Nättilä, M. C. Miller, A. W. Steiner, J. J. E. Kajava, V. F. Suleimanov & J. Poutanen. *ArXiv e-prints*. (2017). (See pp. 50, 52)
"Neutron star mass and radius measurements from atmospheric model fits to X-ray burst cooling tail spectra".

[147]   W. Penninx, E. Damen, J. van Paradijs, J. Tan & W. H. G. Lewin. *A&A*. 208, pp. 146–152. (1989). (See p. 51)
"EXOSAT observations of the X-ray burst source 4U 1608-52".

[148]   J. van Paradijs, T. Dotani, Y. Tanaka & T. Tsuru. *PASJ*. 42, pp. 633–660. (1990). (See pp. 51, 52)
"A very energetic X-ray burst from 4U 2129 + 11 in M15".

[149]   T. Ebisuzaki. *PASJ*. 39, pp. 287–308. (1987). (See p. 52)
"X-ray spectra and atmospheric structures of bursting neutron stars".

[150]   F. Özel. *Nature*. 441, pp. 1115–1117. (2006). (See p. 52)
"Soft equations of state for neutron-star matter ruled out by EXO 0748–676"
DOI: 10.1038/nature04858.

[151]   F. Özel, D. Psaltis, T. Güver, G. Baym, C. Heinke & S. Guillot. *ApJ*. 820, p. 28. (2016). (See p. 52)
"The Dense Matter Equation of State from Neutron Star Radius and Mass Measurements"
DOI: 10.3847/0004-637X/820/1/28.

[152]   V. Suleimanov, J. Poutanen, M. Revnivtsev & K. Werner. *ApJ*. 742, p. 122. (2011). (See p. 52)
"A Neutron Star Stiff Equation of State Derived from Cooling Phases of the X-Ray Burster 4U 1724-307"
DOI: 10.1088/0004-637X/742/2/122.

[153]   J. Poutanen, J. Nättilä, J. J. E. Kajava, O.-M. Latvala, D. K. Galloway, E. Kuulkers & V. F. Suleimanov. *MNRAS*. 442, pp. 3777–3790. (2014). (See p. 52)
"The effect of accretion on the measurement of neutron star mass and radius in the low-mass X-ray binary 4U 1608-52"
DOI: 10.1093/mnras/stu1139.

[154]   V. F. Suleimanov, J. Poutanen, J. Nättilä, J. J. E. Kajava, M. G. Revnivtsev & K. Werner. *MNRAS*. 466, pp. 906–913. (2017). (See p. 52)
"The direct cooling tail method for X-ray burst analysis to constrain neutron star masses and radii"
DOI: 10.1093/mnras/stw3132.